Q-Band MIMO Antennas with Circular Polarization for Spatial and Polarization Diversity

Nada Alaa[1] · Rania A. Elsayed[1] · Asmaa E. Farahat[2] · Khalid F. A. Hussein[2] · Walid S. El-Deeb[1]

Abstract

The present work proposes three MIMO antennas with different configurations for the future applications of wireless communications in the Q-band of the frequency to realize both spatial and polarization diversities. A circularly polarized (CP) printed antenna operating over two frequency bands at 37.8 and 50 GHz is utilized as a single element to construct the proposed MIMO antennas. Two-element MIMO antenna systems arranged in two configurations, side-by-side and face-to-face, are proposed to achieve spatial diversity. Also, a four-element MIMO antenna system is designed to achieve polarization diversity in addition to spatial diversity. The proposed MIMO antenna systems are designed with the aid of the CST simulator. The three MIMO antennas are fabricated and their performance is experimentally evaluated regarding the circular polarization, impedance matching, antenna gain, envelope correlation coefficient (ECC), and diversity gain (DG). The experimental results for the single-element as well as the MIMO antennas come in good agreement with simulation results showing high performance. Both the numerical and experimental investigations reveal that the mutual coupling between any two ports of the proposed MIMO antennas is below -25dB. Also, for any two ports it is shown that the ECC is below 1×10^{-7} and the diversity gain is higher than 9.99. The impedance matching bandwidths (for $|S_{11}| < -10$dB) are shown to be 1.53 and 1.88 GHz at 37.8 and 50GHz, respectively, and the corresponding 3-dB axial ratio bandwidths are 700 and 130MHz, respectively.

Extended author information available on the last page of the article

Springer

1 Introduction

Multiple input multiple output (MIMO) antenna systems employ multiple radiating elements at the transmitter and the receiver. In MIMO system, the transmitter sends data over different multipath propagation then the receiver combines these data through multipath. The main constraint in MIMO antenna system is the uncorrelated multipath which can be provided by using antenna elements acting independently. The MIMO technique provides uncorrelated multipath propagation to attain different diversity schemes. A variety of diversity schemes can be realized such as spatial (space) [1], polarization [2], frequency, pattern (angular) [3–5], and transmit/receive diversity. Employing a dual-band antenna system is preferred to employing two antenna systems operating at two different frequencies because it provides a more compact solution especially for mobile handsets. On the other hand, the circular polarization is preferred for a mobile handset antenna because it allows receiving the power of the incoming signal whether it is circularly polarized (CP) or linearly polarized (LP) without being affected by the misalignment between the transmitting and the receiving antennas. The forthcoming generations of mobile handset need advanced features such as wide bandwidth, high data rate, multiple frequency operation, compact size, and light weight [6–8].

Recently, many research papers [9, 10] focus on the design of mobile handset MIMO antennas for millimeter-wave communications. The work of [11] presents a two-port triple-band MIMO antenna of two elements where each has a single stub that can be embedded in the feed line. There are four symmetric square slots and two cuts in the ground plane to realize circular polarization. The obtained radiation patterns are quasi-omnidirectional. In [12], a dual-band dual-polarized (DBDP) MIMO antenna is designed by using square patch with three rectangular slits and a decoupling mechanism is embedded in the ground structure to enhance the isolation. The non-diagonal slit is responsible for circular polarization. This design is based on the single-feed dual-band antenna and the dual polarization is realized by using an orthogonal feed. There is another category based on using stacked structure that consists of two elements operating at two different frequency bands. In [13], a penta-band MIMO antenna is introduced by adding meander line-shaped radiator with L-shaped matching stub, and ground plane having semi-circle-shaped slot, and inverted L-shaped stub. The proposed four-element MIMO has circular polarization in only two bands. The isolation technique used in design is the inverted L-shaped decoupling structure. In [1], circularly polarized four-element MIMO dielectric resonator antenna (DRA) operating at two frequency bands is studied. We aim to achieve some objectives such as bandwidth enhancement by using a ring-shaped ceramic radiator, dual bands by using incorporation of a rectangular aperture lead, circular polarization by using conversion of rectangular to Z-shaped slot, and reduction of mutual coupling by using space diversity. The work of [14] illustrates the DRA technique for two-port dual-band MIMO antenna with circular polarization. For exciting HE modes, two probes placed orthogonal, that is, an azimuthal angular distance

of 90°, to each other are used. Moreover, to realize the required quadrature time-phase between these modes, the length of two probes must be tuned. The two ring DRAs are excited by using two arc-shaped feed lines with four conformal probes. In [15], a dual-band circularly polarized dielectric resonator antenna is used to implement two-port MIMO antenna that consists of a moon-shaped aperture. To stimulate ring-shaped DRA, L-shaped microstrip line with a serial step imped-ance transformer is used. Modification from cylindrical to ring-shaped dielec-tric resonator provides wide impedance bandwidth. Aperture is helpful to excite the dual orthogonal hybrid modes for circular polarization waves. Polarization diversity is supportive to reduce the mutual coupling between ports. A broadband antenna operating over the 38 GHz frequency band is proposed in [16], using cir-cular patch antenna loaded by three patches between circular radius and feed-line and perpendicular pair of elliptical slots inside the circular patch. This antenna has small size with 7-dB gain and 90% radiation efficiency. In [17] and [18], a compact multiband antenna operating at 28, 38, and 55 GHz is introduced. The antenna has an umbrella-shaped patch with high gain and efficiency. A wideband, high-gain, low-profile, and high-efficiency fractal antenna operating at 39 GHz is investigated in [19]. The antenna is designed on a Rogers RT/duroid 5880 with a compact size of $15 \times 15 \times 0.79$ mm.

This work introduces two-element as well as four-element MIMO antenna systems to achieve spatial diversity as well as polarization diversity for millim-eter wave (mm-wave) applications. A dual-band circularly polarized (DBCP) microstrip patch antenna is used as a single element to construct the proposed MIMO antennas. The single element is designed as a main patch and a para-sitic patch. The main patch has circular geometry with two square slots at the center and two notches on the circumference. The parasitic patch consists of four parasitic elements indirectly fed by capacitively coupling to the main patch. To produce circular polarization, the structure of the single element antenna is sym-metric about an axis that is inclined to the feed line at angle of 45°. For imped-ance matching, the main patch is fed through a microstrip line with tapered geometry.

Two-element MIMO antenna systems are proposed to produce spatial diver-sity: face-to-face and side-by-side arrangements. The four-element MIMO antennas are proposed to produce both spatial and polarization diversity at the same time. If the elements have the same sense of polarization, then spatial diversity is obtained, whereas polarization diversity is obtained if the elements have different senses of polarization. The proposed MIMO antenna systems have two operational frequency bands centered at 38 and 50 GHz and produce circular polarization over the two frequency bands. The diversity schemes pro-vided by these MIMO antennas are investigated by the CST simulator where the envelope correlation coefficient (ECC) and the diversity gain (DG) are investigated and demonstrated.

The presentation of this work is organized as follows. Section 2 presents the design of the single-element dual-band CP antenna. Section 3 introduces the pro-posed MIMO antennas with the different configurations. Section 4 describes the fab-rication process and the experimental setup for measurements. Section 5 presents

the simulation and experimental results with elaborate discussions for performance assessment. Section 6 introduces a summary of this work and some comparisons to the achievements of the other published papers. Finally, Section 7 gives the conclusions related to the present work.

2 Design of Single-Element Antenna

The geometry of the CP patch antenna proposed as a single element for the two-element and four-element MIMO antenna systems is depicted in Fig. 1. This antenna consists of a circular patch that acts as the main radiator which is reactively loaded by four parasitic patches as seen in Fig. 1a. To produce circular polarization, two square slots are made near the patch center and two notches are etched at the patch edge to get the line of symmetry of the antenna structure having a slope of 45° with the center line of the feeding microstrip line. Also, the ground structure is defected by etching two square slots as shown in Fig. 1b. Thus, the overall patch and defected ground geometry have a line of symmetry making 45° with the center line of the microstrip line feeder. This symmetry produces two degenerate radiating modes (resonances) of the cavity between the circular patch and the ground plane. The radiated fields of the two modes have nearly equal magnitudes, orthogonal orientations, and in-phase quadrature; these conditions produce a circularly polarized field in the far zone of the antenna. The antenna's geometrical parameters should be set to the appropriate values to satisfy these conditions. The antenna impedance is matched at the desired frequencies by the tapered microstrip line feeder. The dimensions of the tapered region of this line, W_T, L_T, and W_F, should be set to get the antenna impedance matched to 50Ω source at the required frequencies. The parasitic elements help to get the antenna impedance matched over a higher frequency band. The Y-shaped slits at the corners of the parasitic elements improve the axial ratio and increase its 3-dB bandwidth. The geometric symmetry of the antenna around an axis inclined to the feed line at an angle of 45° produces right-hand circularly polarized (RHCP) field in the far zone. If this geometry is mirrored about the centerline of the microstrip feeder, left-hand circularly polarized (LHCP) fields are produced in the far zone. It will be shown, later, that two antennas of opposite senses of polarization can be used in a four-element MIMO antenna configuration to provide polarization diversity in addition to the spatial diversity.

The optimal dimensions of this antenna are listed in Table 1. It should be noted that these dimensions have been obtained through an extensive parametric study that has been achieved using the CST simulator. The proposed MIMO is designed using a substrate material of the type Rogers RO3003. The substrate has a thickness $h = 0.25$mm, loss tangent tan$\delta = 0.001$, and dielectric constant $\varepsilon_r = 3$.

In this section, two-element and four-element configuration of MIMO antenna systems are proposed to produce spatial and polarization diversity. The design of the proposed MIMO antennas are presented in the following subsections.

(a)

(b)

(c)

(d)
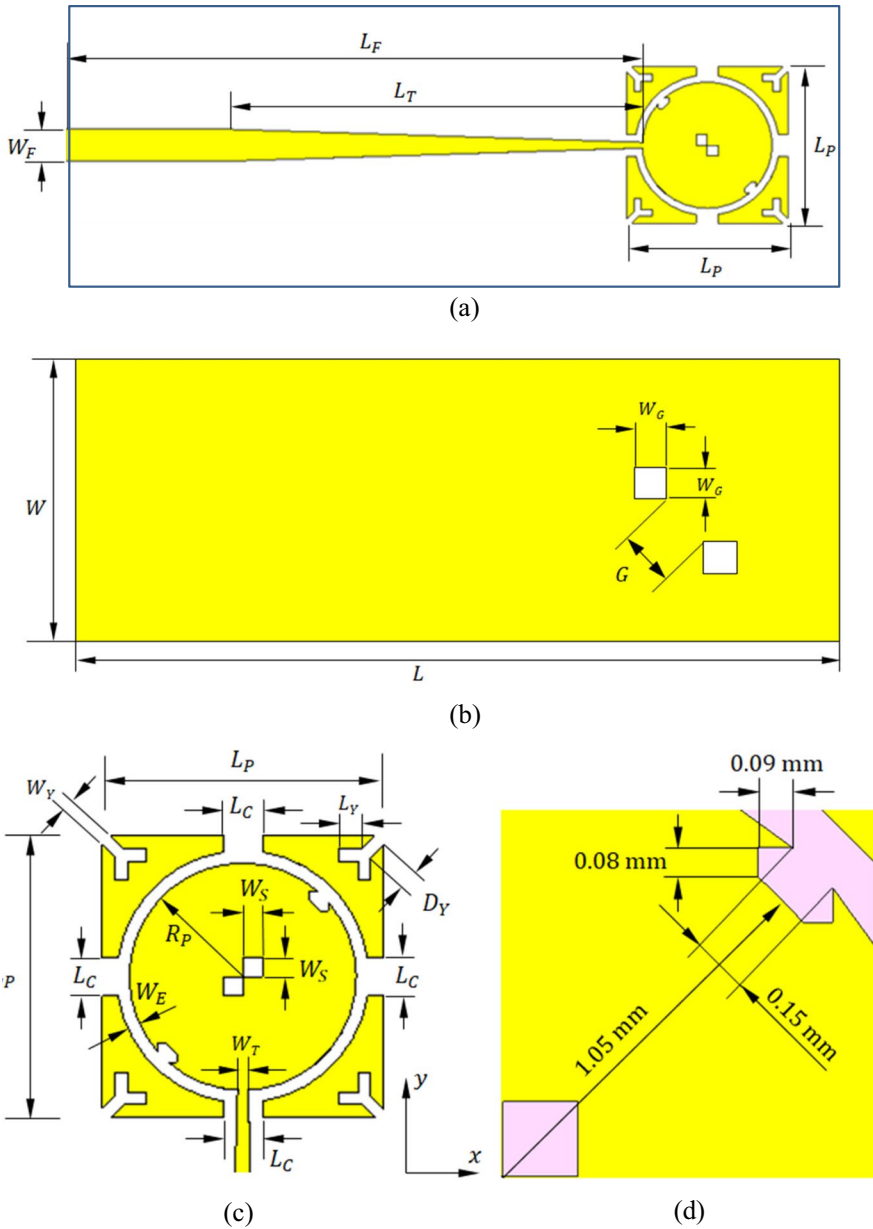
Fig. 1 Structure of the dual-band circularly polarized single-element patch antenna. **a** Top view. **b** Bottom view. **c** Detailed view of the patch. **d** Close view at one notch on the patch circumference

Table 1 Optimum values of the dimensions of the single-element antenna proposed for different MIMO antenna configurations

Dimension	R_P	L_P	W_F	L_F	W_T	L_T	W_G	G	W_E	W_S	L_C	W_Y	L_Y	D_Y
Value (mm)	1.17	2.9	0.6	11.05	0.1	7.6	0.6	1.414	0.13	0.2	0.4	0.13	0.2	0.18

3 Proposed MIMO Antenna Systems

In this section, the designs of the proposed MIMO antennas are described in detail. Two-element MIMO antennas arranged in side-by-side and face-to-face configurations are designed to produce spatial diversity. Also, four-element MIMO antenna system is designed to produce both spatial and polarization diversity. The following two subsections are dedicated for the description of the different types of the proposed MIMO antenna configurations.

3.1 Two-Port MIMO Antenna Configurations for Spatial Diversity

Two configurations are proposed to construct two-element MIMO antennas by using the CP patch described in Section 2. In the first configuration, the patch antennas are arranged side-by-side, whereas in the other configuration, the two patch elements are arranged face-to-face as shown.

For two-element MIMO antenna, the ECC can be expressed as follows [20]:

$$ECC_{1,2} = \frac{\left|S_{11}^* S_{12} + S_{21}^* S_{22}\right|^2}{(1 - |S_{11}|^2 - |S_{12}|^2)(1 - |S_{21}|^2 - |S_{22}|^2)^*} \quad (1)$$

For two-element MIMO antenna, the DG can be expressed as follows [20]:

$$DG = 10\sqrt{1 - |ECC|^2} \quad (2)$$

Each of the proposed two-element MIMO antenna configurations may have different performance from the other and both are investigated in the present work. The next two subsections are dedicated to describe the designs of the proposed two-element MIMO configurations.

3.1.1 Two-Element MIMO Antenna in Side-by-Side Configuration

In the two-element side-by-side MIMO antenna configuration, the patch antennas are arranged as shown in Fig. 2. If the two elements in this MIMO antenna configuration have the same sense of polarization, then spatial diversity is produced. If an element is LHCP whereas the other element is RHCP, then polarization diversity is
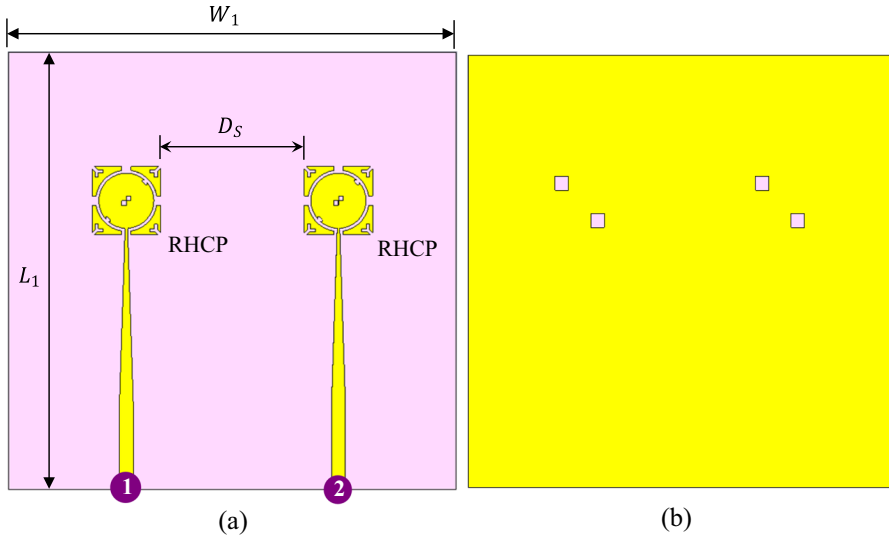
Fig. 2 Design of the two-element side-by-side MIMO antenna using two elements of the dual-band circularly polarized antenna. **a** Top view. **b** Bottom view
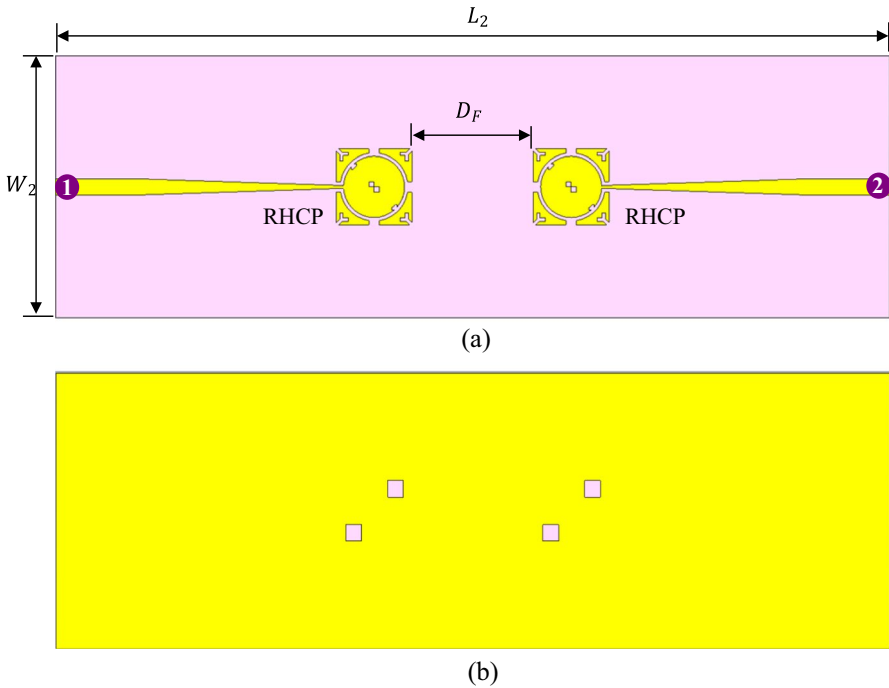
Fig. 3 Design of the two-element face-to-face MIMO antenna using two elements of the dual-band circularly polarized antenna. **a** Top view. **b** Bottom view

produced. In this MIMO antenna, the elements are printed on the same substrate. The overall physical dimensions of the two-element side-by-side MIMO antenna are $L_1 = 19$mm and $W_1 = 18.5$mm. The spacing between the antenna elements is $D_S = 6.1$mm.

3.1.2 Two-Element MIMO Antenna in Face-to-Face Configuration

In the two-element face-to-face MIMO antenna configuration, the patch antennas are arranged as shown in Fig. 3. If the two elements in this MIMO antenna configuration have the same sense of polarization, then this MIMO antenna produces spatial diversity. If an element is LHCP whereas the other element is RHCP, then polarization diversity is produced. In this MIMO antenna, the elements are printed on the same substrate. The overall physical dimensions of the two-element face-to-face MIMO antenna are $L_2 = 32$mm and $W_2 = 10$mm. The spacing between the antenna elements is $D_F = 4.66$mm.

3.2 Four-Element MIMO Configuration for Both Spatial and Polarization Diversity

Four elements of the dual-band CP antenna, described in Section 2, are arranged as shown in Fig. 4 to implement the proposed MIMO antenna system. To obtain polarization diversity in addition to the spatial diversity by such four-element MIMO antenna, elements 1 and 4 are RHCP, whereas elements 2 and 3 are LHCP. In this way, both spatial and polarization diversities are obtained. The separation distances between the elements are $D_S = 6.1$mm and $D_F = 4.66$mm. The total dimensions of the four-element MIMO antenna are $L_3 = 32$mm and $W_3 = 18.5$mm.

4 Fabrication and Experimental Setup for Measurements

Prototypes are fabricated for experimental evaluation of the proposed single-element and MIMO antennas' performance. The reflection coefficient at the antenna input ports and the radiation patterns are measured and compared to the simulation results.

4.1 Fabricated Prototypes

Prototypes are fabricated for the single-element, two-element side-by-side MIMO, two-element face-to-face MIMO, and four-element MIMO antennas whose designs are presented in Figs. 1, 2, 3, and 4, respectively. The fabricated prototypes are presented in Fig. 5. The elements of the MIMO antennas are fed at each port through 1.85-mm coaxial end launchers from Southwest Microwave Inc. The purpose of fabricating these prototypes is the experimental evaluation of the antenna performance for comparison with the simulation results.
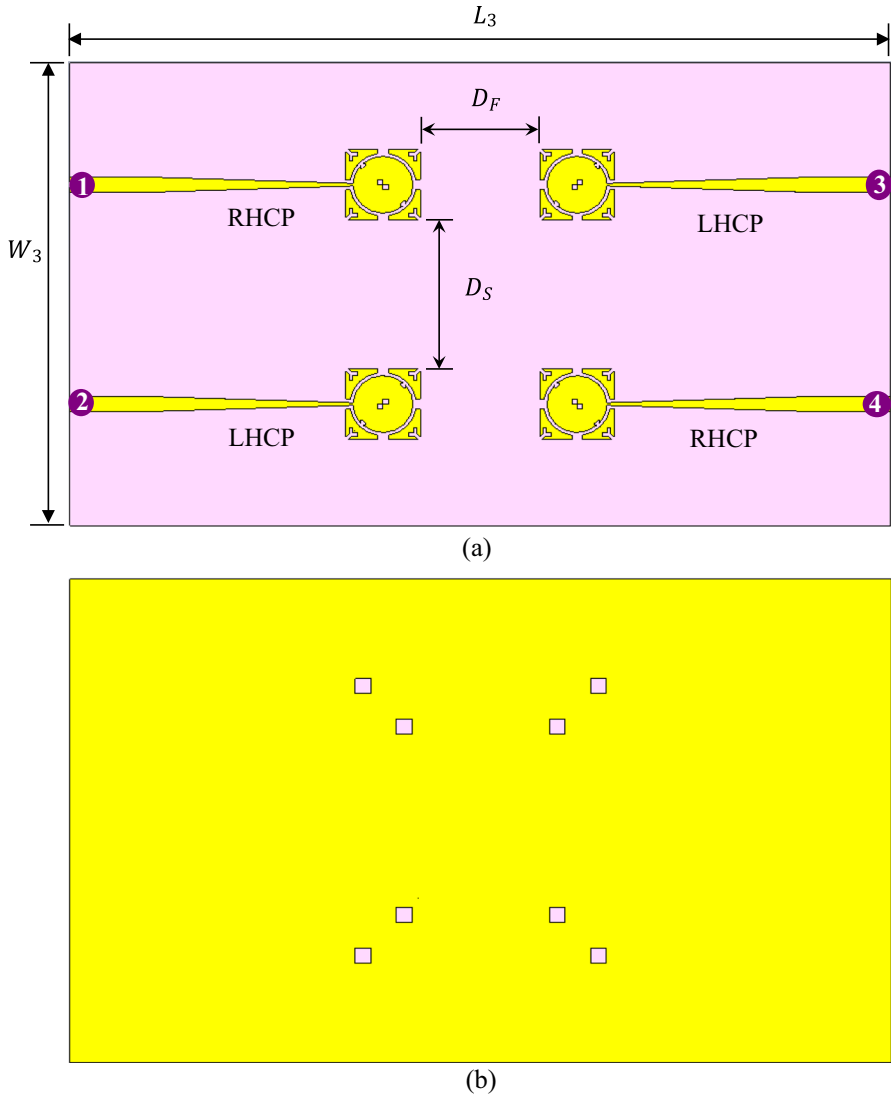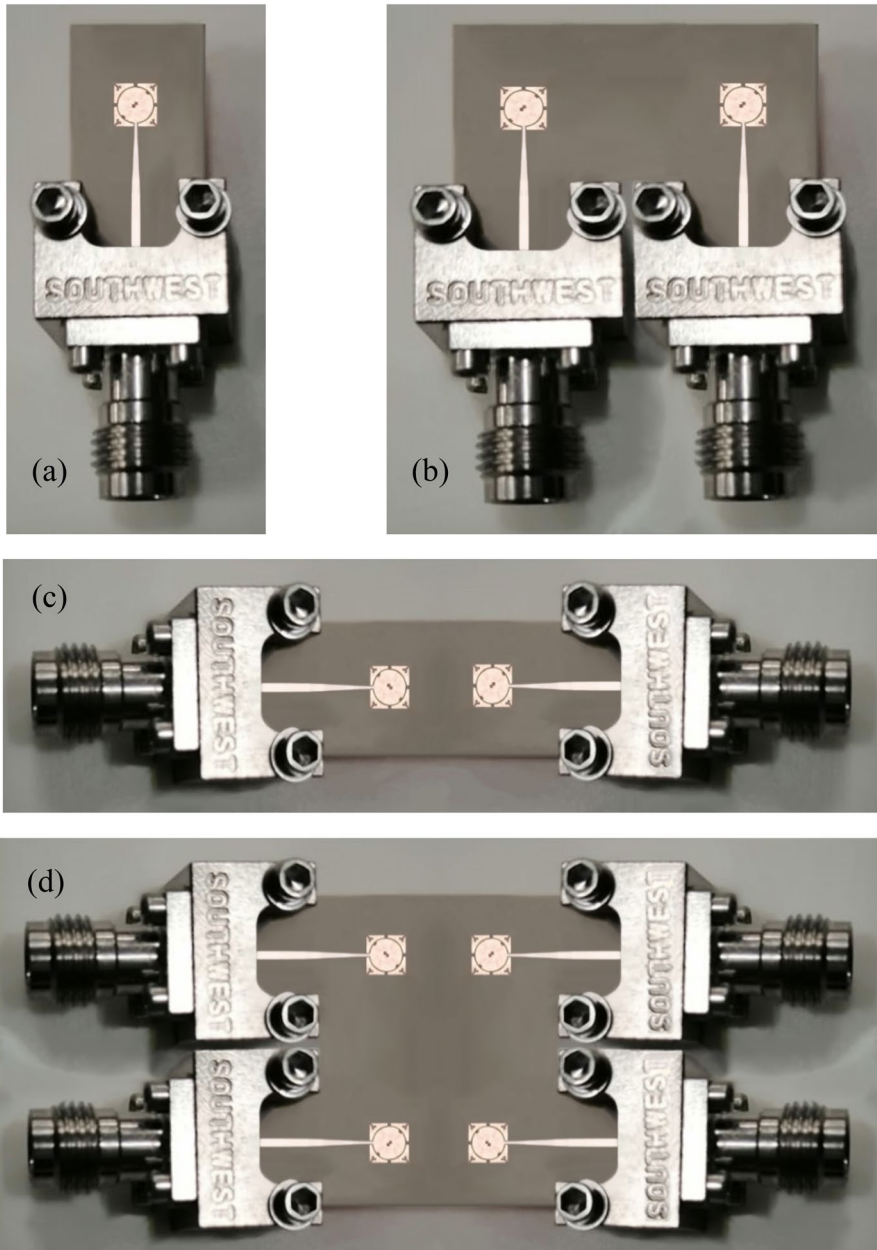
Fig. 4 Design of the four-element MIMO antenna system using four dual-band circularly polarized patch antennas. **a** Top view. **b** Bottom view

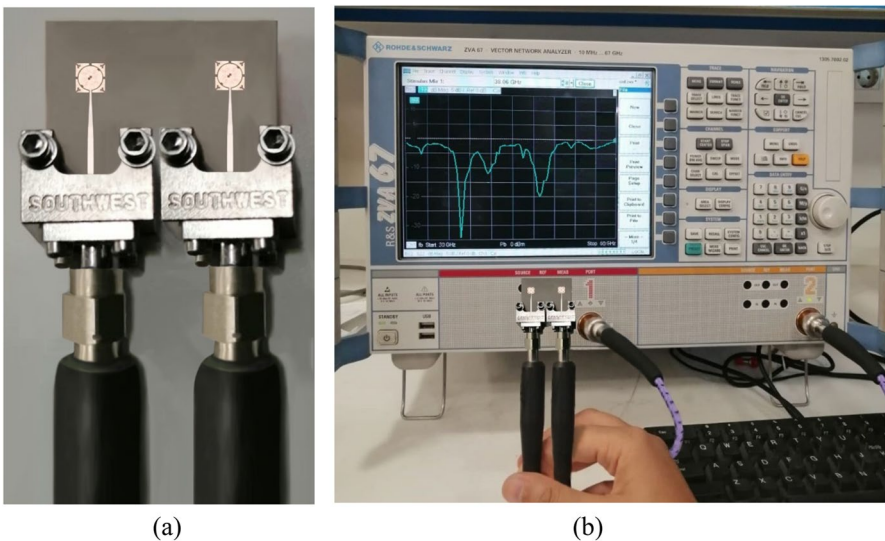## 4.2 Measurement of the Self and Mutual Scattering Parameters

The self and mutual scattering parameters are measured with the aid of the VNA model Rhode and Schwartz ZVA67. The end-launch connectors of type 1.85mm from Southwest Microwave Inc. are used to connect the antennas under test to the VNA for measurement as shown in Figs. 6 and 7.

Fig. 5 Fabricated prototypes of the proposed antennas. **a** Single element. **b** Two-element side-by-side MIMO antenna. **c** Two-element face-to-face MIMO antenna. **d** Four-element MIMO antenna

(a)   (b)
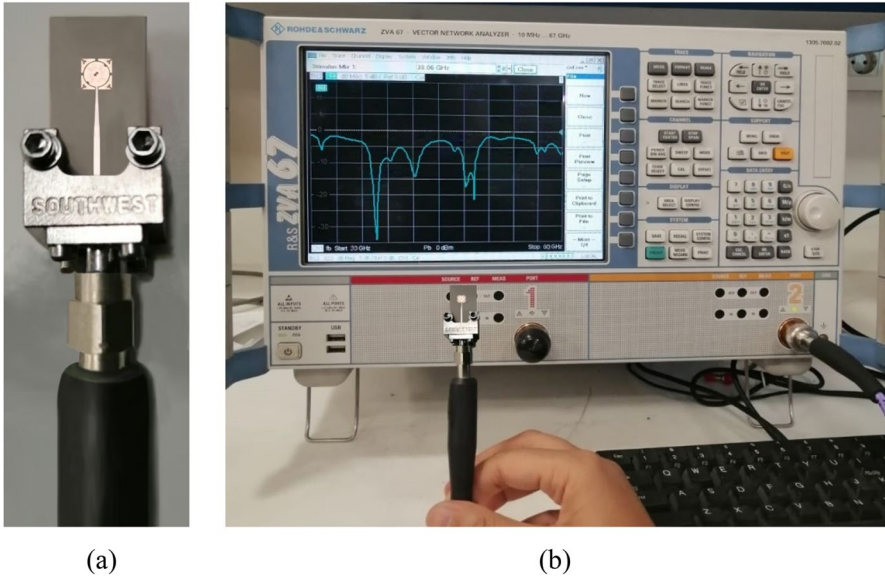
Fig. 6 Measurement of the *S*-parameter, S_{11}, of the fabricated single-element antenna. **a** The antenna connected to the VNA cable via the end-launch connector. **b** Experimental setup showing the antenna connected to port 2 of the VNA

(a)   (b)

Fig. 7 Measurement of the *S*-parameters, S_{11}, S_{22}, and S_{21}, of the two-element side-by-side fabricated prototypes. **a** Two fabricated elements arranged side-by-side and connected to the VNA cables via the end-launch connectors. **b** Experimental setup showing two-element MIMO antenna connected to ports 1 and 2 of the VNA
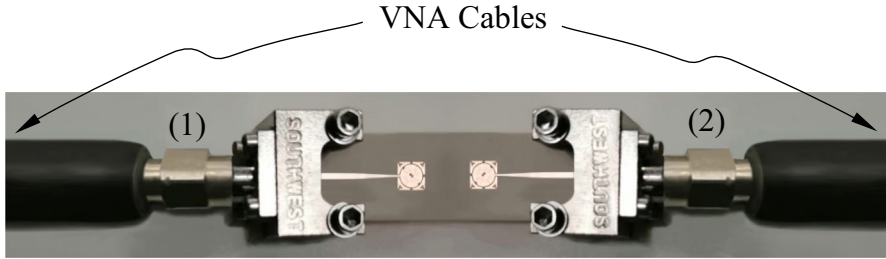
Fig. 8 The fabricated two-element face-to-face MIMO antenna is prepared for measuring the self and mutual scattering parameters, S_{11}, S_{22}, and S_{21}
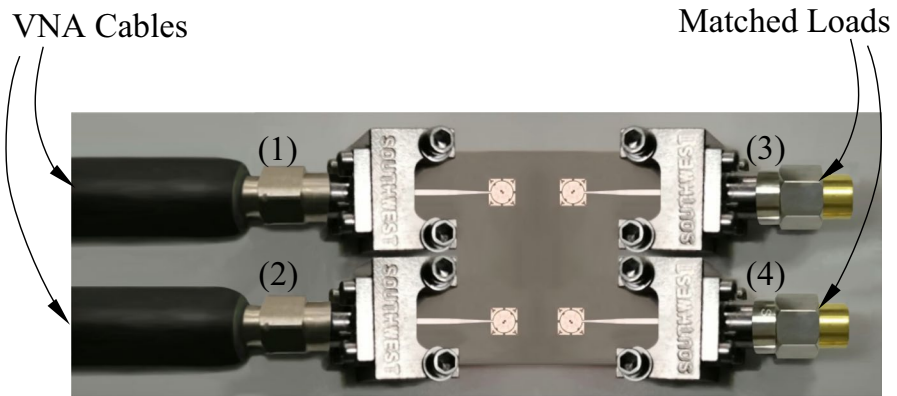
Fig. 9 The fabricated four-element MIMO antenna is prepared for measuring the self and mutual scattering parameters, S_{11}, S_{22}, and S_{21}. The VNA cables are connected to ports 1 and 2 and matched loads are connected to ports 3 and 4 of the MIMO

The fabricated prototypes of the two-element (face-to-face) and the four-element antennas are prepared for measuring the self and mutual the *S*-parameters, S_{11}, S_{22}, and S_{21}, as seen in Figs. 8 and 9, respectively.

4.3 Measurement of the Radiation Patterns

The gain and radiation patterns of the proposed single-element and MIMO antennas are measured by the aid of the VNA. The experimental setup is presented in Fig. 10 showing the reference gain linearly polarized horn antenna mounted on the polarization rotator, the antenna-under-test (AUT) mounted on the directional rotator. The horn antenna model LB-018400 is employed to perform measurements over the frequency range of 18–40 GHz while the horn antenna model LB-12–10-A is employed to perform measurements over the frequency range of 40–60 GHz. The AUT and the
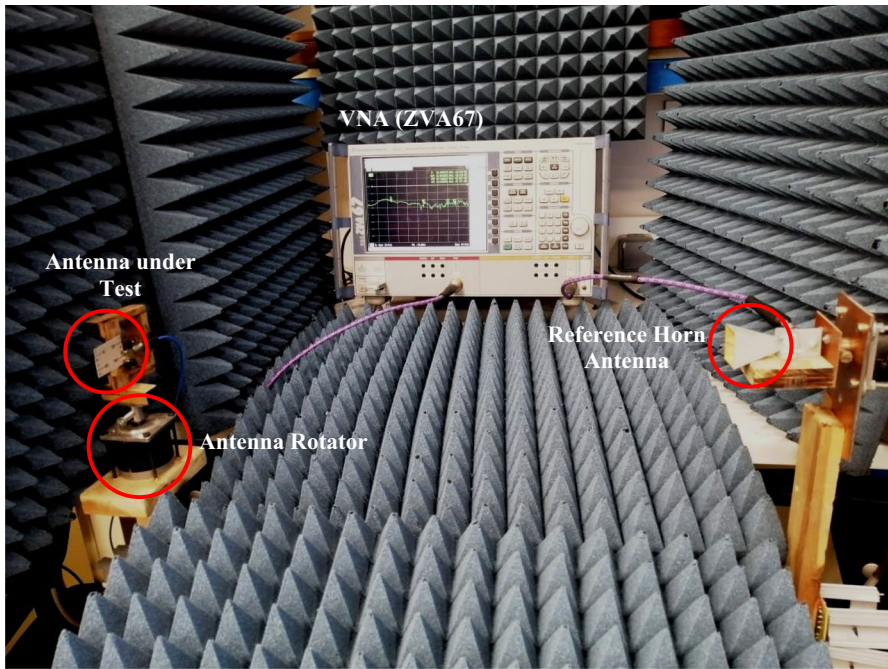
Fig. 10 Gain and radiation pattern pattern measurement setup showing the AUT and reference horn antenna connected to ports 1 and 2 of the VNA, respectively
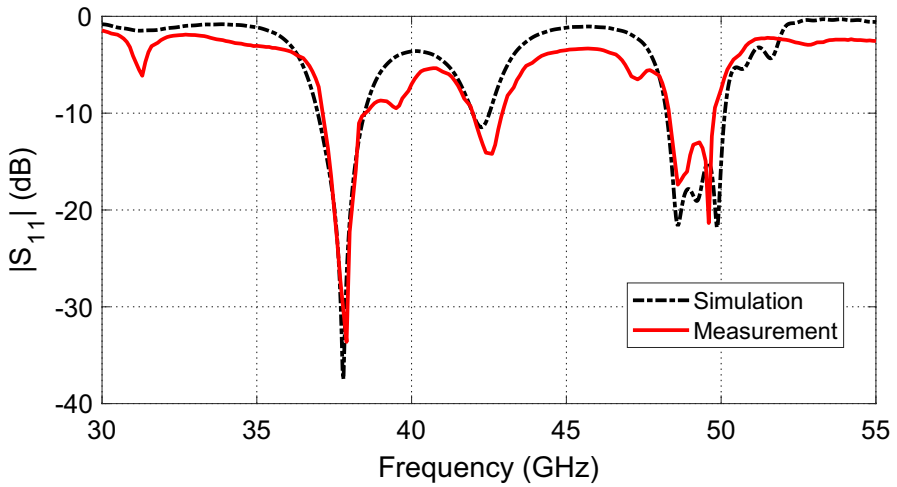
Fig. 11 Results of simulation and measurement of the reflection coefficient magnitude, $|S_{11}|$, at the feeding port of the single-element antenna over a broad frequency band

reference-gain horn antenna are connected to ports 1 and 2 of the VNA, respectively. The ratio of the received power to the transmitted power is assessed by the magnitude of the transmission coefficient, $|S_{21}|$, between AUT and the reference antenna.

5 Results and Discussions

The simulation results and experimental measurements are presented and discussed in this section. The main concern of such presentations is the performance evaluation of the single-element antenna as well as the MIMO antennas with the different configurations proposed in the present work.

5.1 Performance Evaluation of the Single-Element Antenna

The frequency dependence of $|S_{11}|$ at the feeding port of the single-element dual-band circularly polarized antenna, described in Section 2, is investigated by simulation as well as experimental measurement at the frequencies ranging from 34 to 54 GHz. Figure 11 shows that the measurements are very close to the simulation results. It is shown that the antenna impedance is perfectly matched to 50Ω over the two frequency bands at 38 and 50 GHz.
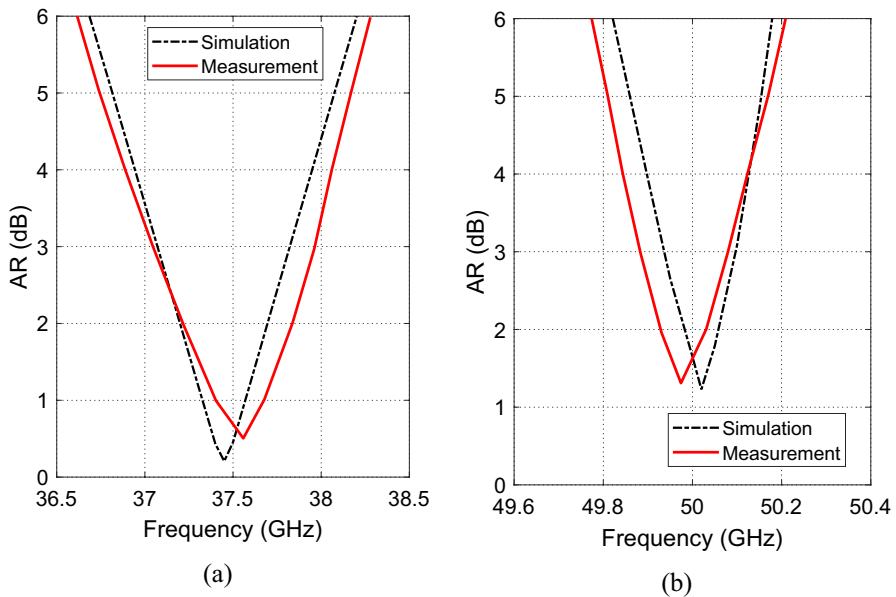
Fig. 12 Results of simulation and measurement of the AR over (**a**) the lower frequency band and (**b**) the higher frequency band
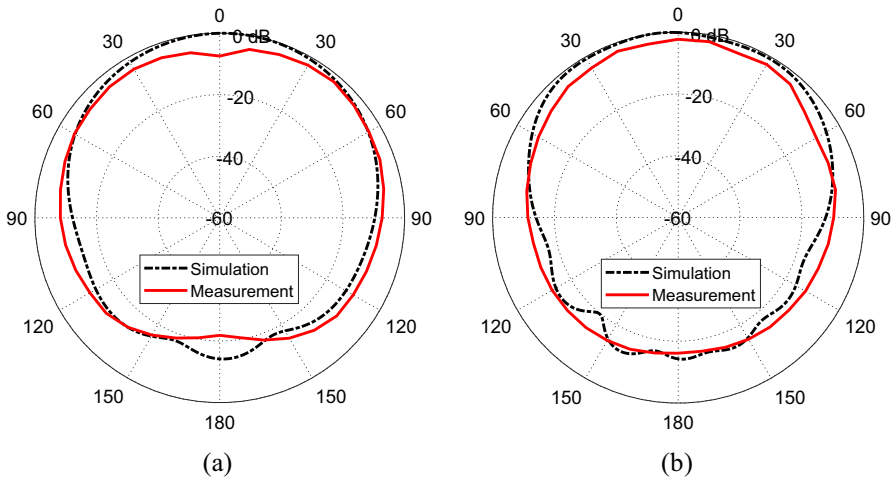
Fig. 13 Total field radiation patterns of the single-element antenna at 37.8GHz. **a** $\phi = 0°$. **b** $\phi = 90°$
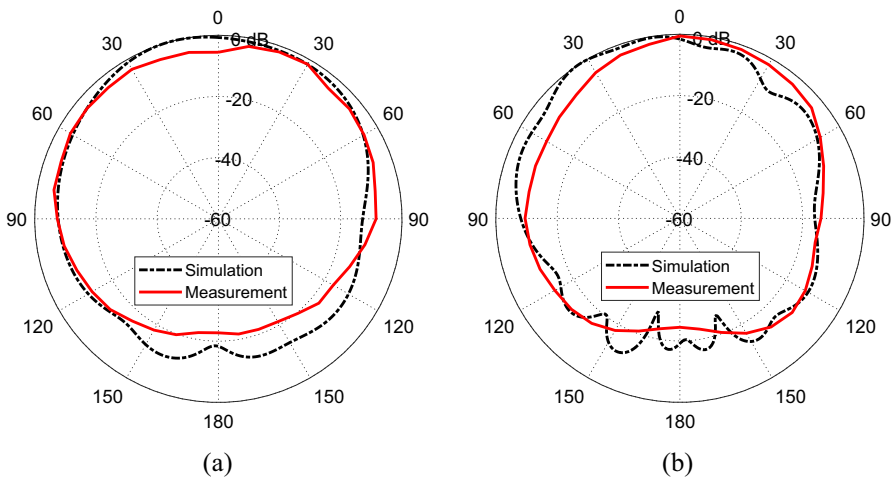
Fig. 14 Total field radiation patterns of the single-element antenna at 50GHz. **a** $\phi = 0°$. **b** $\phi = 90°$

The variations of the AR of the single-element antenna with the frequency around the frequencies 37.8 and 50GHz are presented in Fig. 12a and b, respectively. As shown in these figures, the experimental measurements show excellent agreement with the simulation results. The 3dB-AR bandwidth at 37.8 and 50GHz are 700 and 300 MHz, respectively.

The total far-field radiation patterns of the single-element antenna at 38 and 50 GHz are depicted in Figs. 13 and 14, respectively. The radiation patterns produced at the two frequencies show that this single-element antenna is a good candidate to construct MIMO antenna systems with high performance.
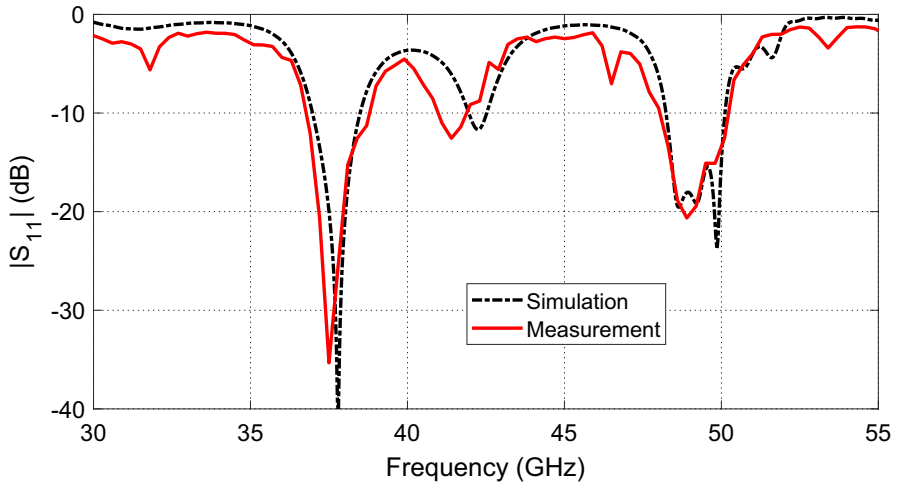
Fig. 15 Results of simulation and measurement of $|S_{11}|$ at port 1 of the two-element side-by-side MIMO antenna over a broad frequency band
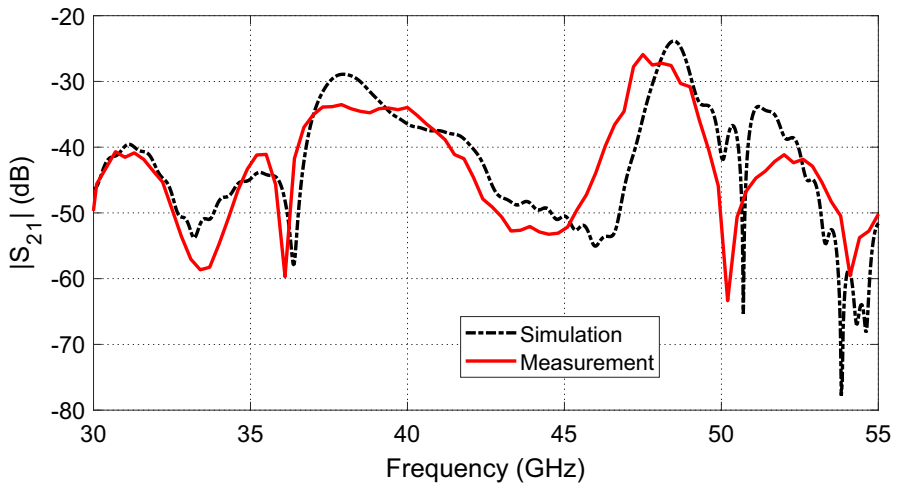
Fig. 16 Results of simulation and measurement of the mutual coupling coefficient, $|S_{21}|$, of the two-element side-by-side MIMO antenna
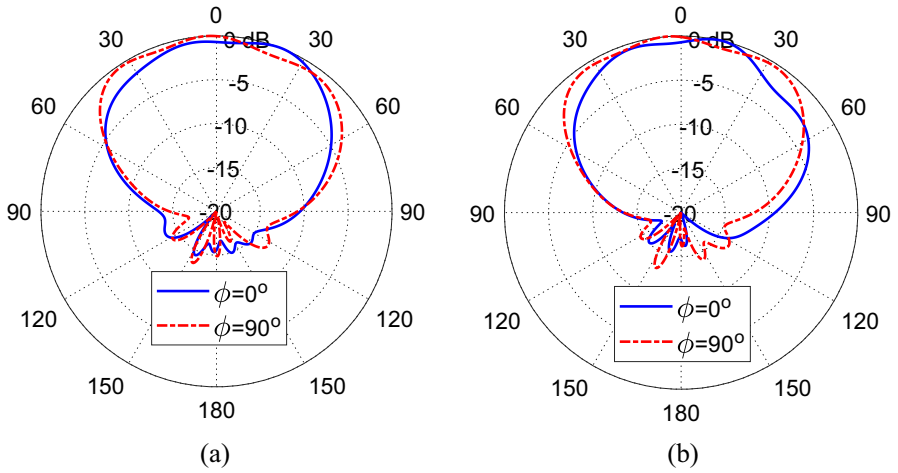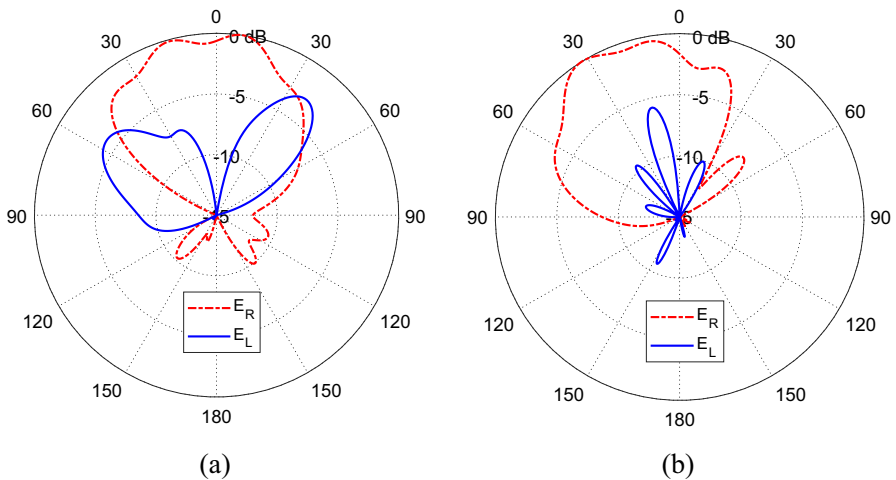
Fig. 17 Total field radiation patterns of the two-element side-by-side MIMO antenna at 37.8GHz when fed at (**a**) port 1 and (**b**) port 2
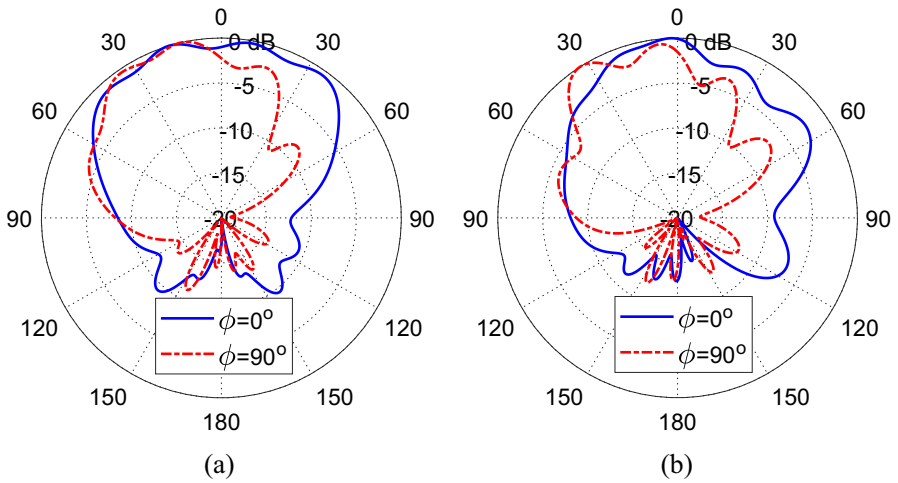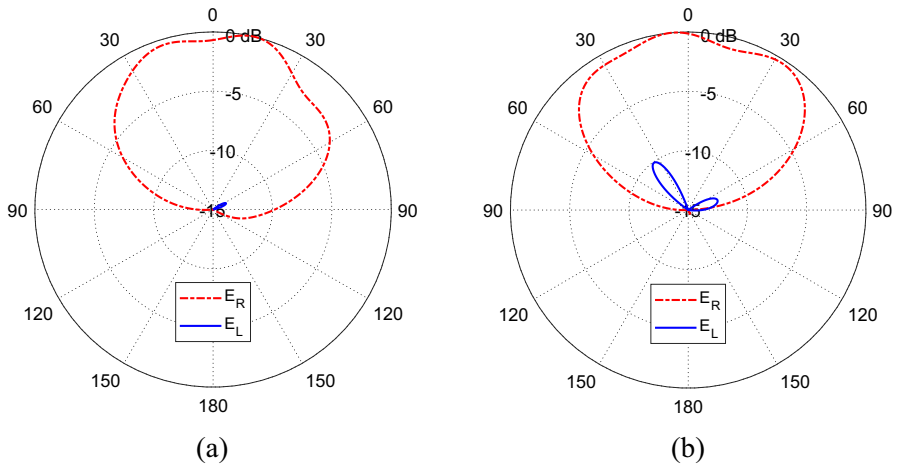

Fig. 18 Total field radiation patterns of the two-element side-by-side MIMO antenna at 50GHz when fed at (**a**) port 1 and (**b**) port 2
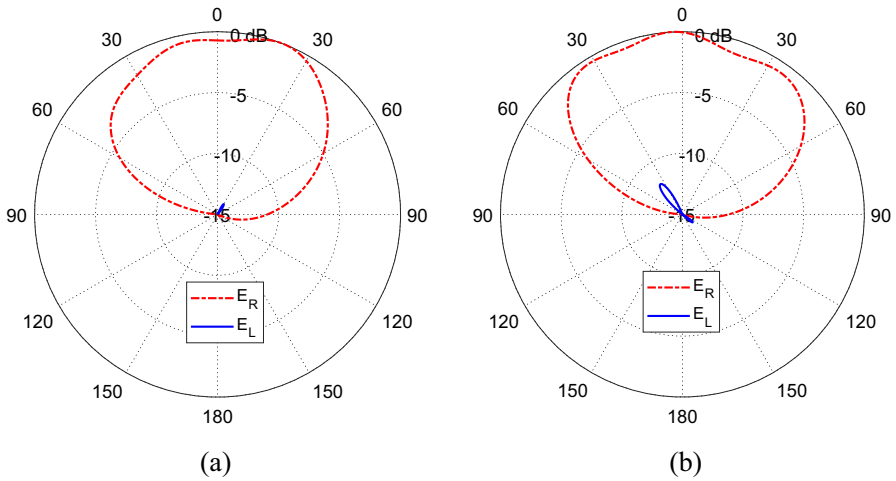
Fig. 19 Radiation patterns of the CP field components (E_R and E_L) of the two-element side-by-side MIMO antenna (port 1) at 37.8 GHz. **a** $\phi = 0°$. **b** $\phi = 90°$

Fig. 20 Radiation patterns of the CP field components (E_R and E_L) of the two-element side-by-side MIMO antenna (port 1) at 50 GHz. **a** $\phi = 0°$. **b** $\phi = 90°$

5.2 Performance Evaluation of the Two-Element MIMO Antennas

The purpose of the next two subsections is to investigate the performance of the two-element MIMO configurations proposed in Section 3.1 regarding the impedance matching at each port, radiation patterns, coupling coefficient between the two ports, ECC, and DG.

Fig. 21 Radiation patterns of the CP field components (E_R and E_L) of the two-element side-by-side MIMO antenna (port 2) at 37.8 GHz. **a** $\phi = 0°$ **b**. $\phi = 90°$
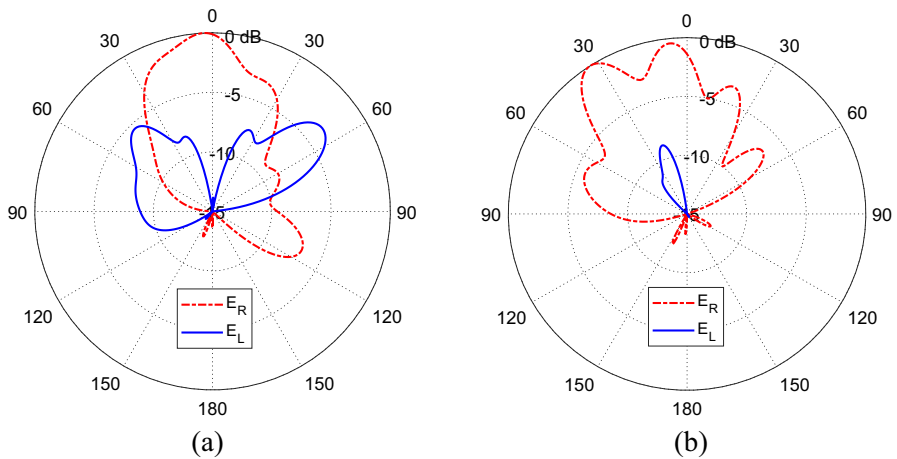
Fig. 22 Radiation patterns of the CP field components (E_R and E_L) of the two-element side-by-side MIMO antenna (port 2) at 50 GHz. **a** $\phi = 0°$. **b** $\phi = 90°$

5.2.1 Two-Element Side-by-Side MIMO Antenna

In this section, the performance of a MIMO antenna system composed of two elements of the antenna described in Section 2 is investigated by simulation as well as experimental measurement. The two elements are placed side-by-side, as presented in Figs. 2 and 5b, to produce spatial diversity. The frequency dependence of the reflection coefficient at port 1 is presented in Fig. 15. By comparison between Figs. 15 and 11, it is shown that the frequency response of $|S_{11}|$ of
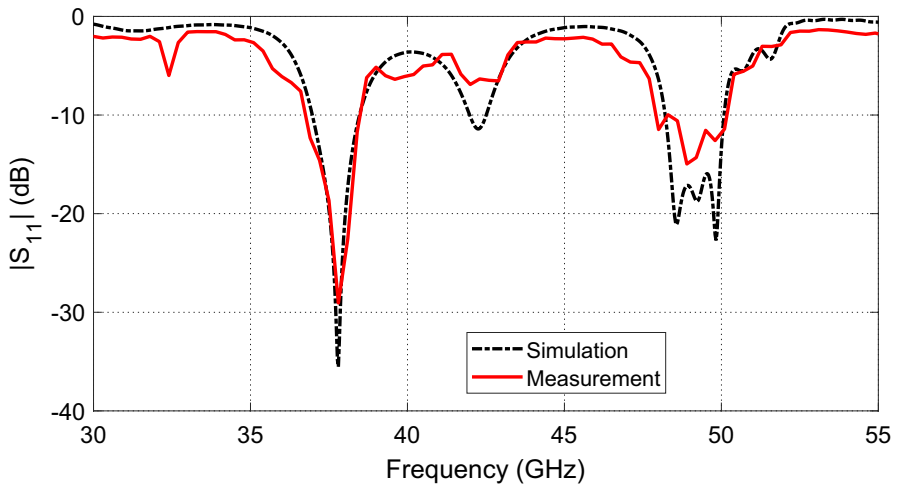
Fig. 23 Results of simulation and measurement of $|S_{11}|$ at port 1 of the two-element face-to-face MIMO antenna over a broad frequency band

the two-element MIMO antenna is almost identical to that of the single-element antenna.

The isolation between the two elements of this MIMO antenna can be measured by the magnitude of the coupling coefficient, $|S_{21}|$, whose frequency response is shown in Fig. 16. The magnitude of this coefficient is maintained below -24 dB over the entire frequency range of investigation showing good performance of the proposed side-by-side MIMO antenna. Also, it is shown that the simulation
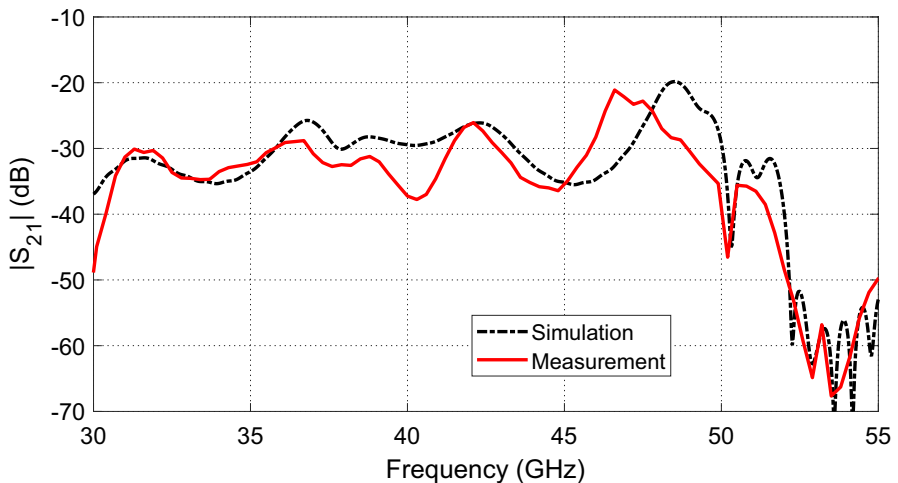

Fig. 24 Results of simulation and measurement of the mutual coupling coefficient, $|S_{21}|$, of the two-element face-to-face MIMO antenna
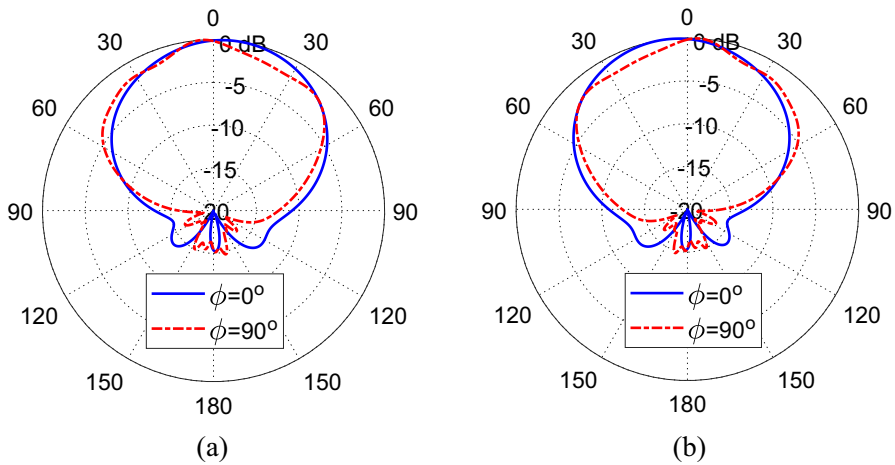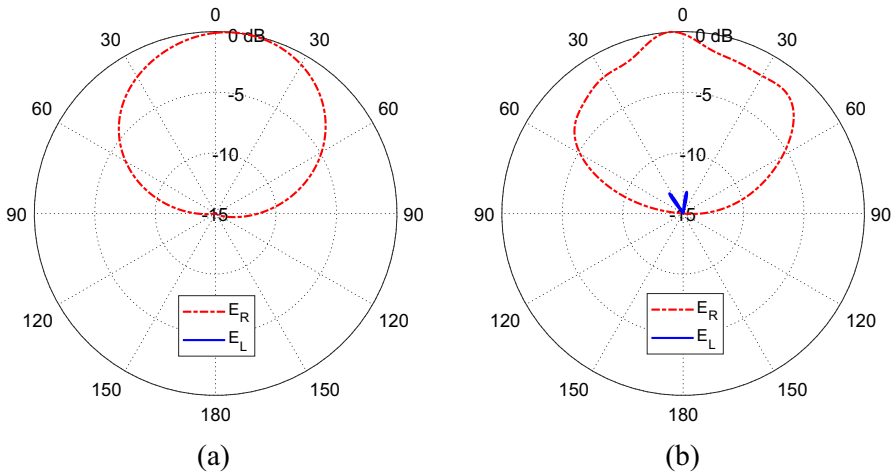
Fig. 25 Radiation patterns of the total field radiated by the two-element face-to-face MIMO antenna at 37.8GHz when it is fed using (**a**) port 1 and (**b**) port 2

results and experimental measurements of $|S_{11}|$ and $|S_{21}|$ show good agreement with each other.
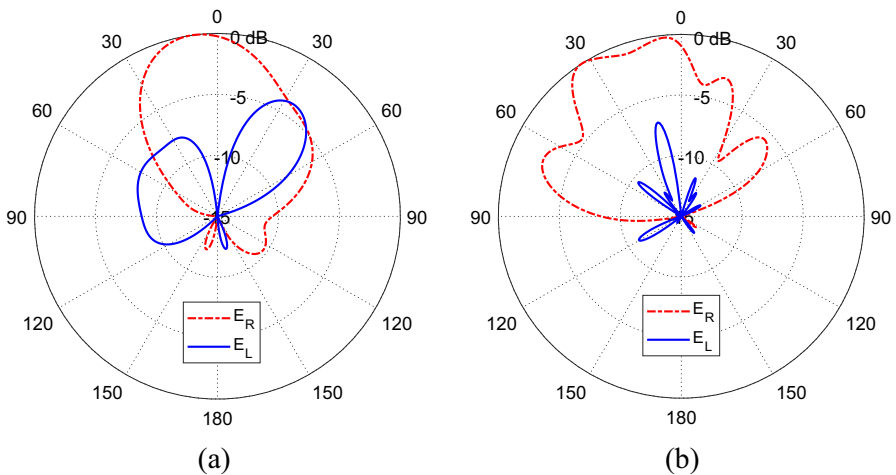
The radiation patterns of the two-element side-by-side MIMO antenna at 37.8 GHz when excited at ports 1 and 2 are presented in Fig. 17a and b, respectively. The far-field patterns produced at 50 GHz when this MIMO antenna is fed at ports 1 and 2 are presented in Fig. 18a and b, respectively. Irrespective of the port of excitation of this MIMO antenna, the values of the maximum gain achieved at 37.8 and 50 GHz are 7 and 6.8 dBi, respectively.
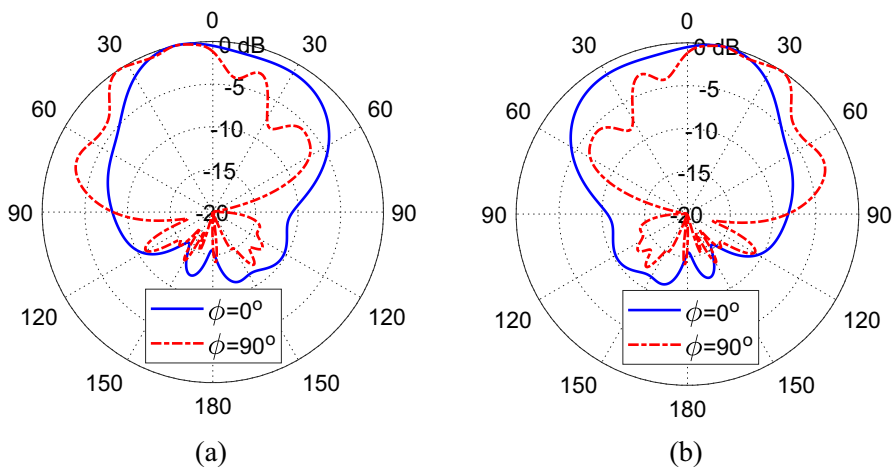
Fig. 26 Radiation patterns of the total field radiated by the two-element face-to-face antenna at 50GHz when it is fed using (**a**) port 1 and (**b**) port 2
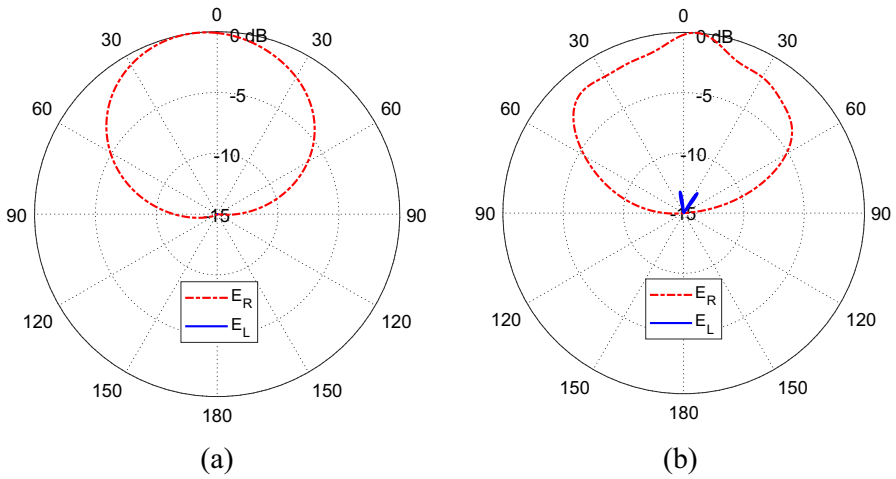
Fig. 27 Radiation patterns of the CP field components (E_R and E_L) of the two-element face-to-face MIMO antenna (port 1) at 37.8 GHz. **a** $\phi = 0°$. **b** $\phi = 90°$

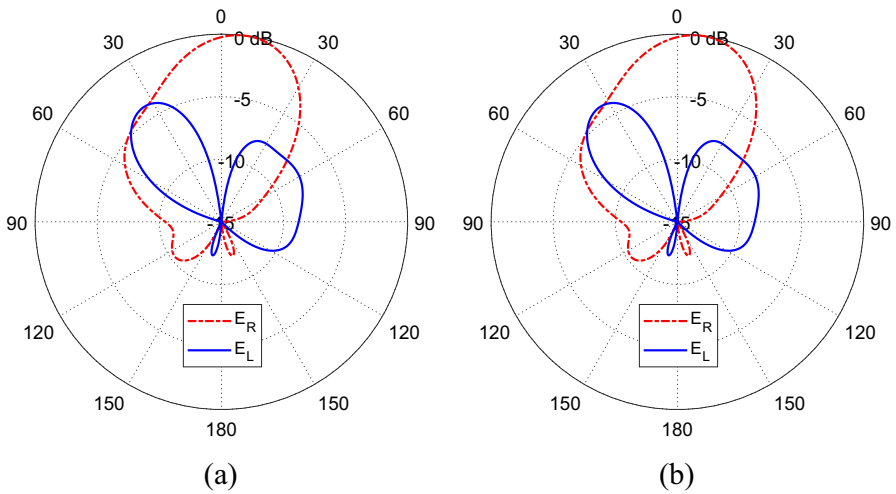

Fig. 28 Radiation patterns of the CP field components (E_R and E_L) of the two-element face-to-face MIMO antenna (port 1) at 50 GHz. **a** $\phi = 0°$. **b** $\phi = 90°$

When the side-by-side MIMO antenna is fed using port 1, the patterns of the CP field components at 37.8 and 50 GHz are presented in Figs. 19 and 20, respectively. When the same MIMO antenna is fed using port 2, the CP field patterns at 37.8 and 50 GHz are presented in Figs. 21 and 22, respectively. It is seen that the radiated field is dominated by RHCP component at both the lower and higher frequencies. However, the cross-polarization level of the radiated field at 50GHz is significantly higher than that of the radiated field at 37.8GHz.

(a)

(b)

Fig. 29 Radiation patterns of the CP field components (E_R and E_L) of the two-element face-to-face MIMO antenna (port 2) at 37.8 GHz. **a** $\phi = 0°$. **b** $\phi = 90°$

(a)

(b)

Fig. 30 Radiation patterns of the CP field components (E_R and E_L) of the two-element face-to-face MIMO antenna (port 1) at 50 GHz. **a** $\phi = 0°$. **b** $\phi = 90°$

This means that the proposed two-element side-by-side MIMO antenna produces more perfect circular polarization at 37.8 GHz that that produced at 50 GHz. This MIMO antenna produces the same type of polarization when fed using port 1 or port 2. Therefore, it can be employed to obtain spatial diversity but not polarization diversity.
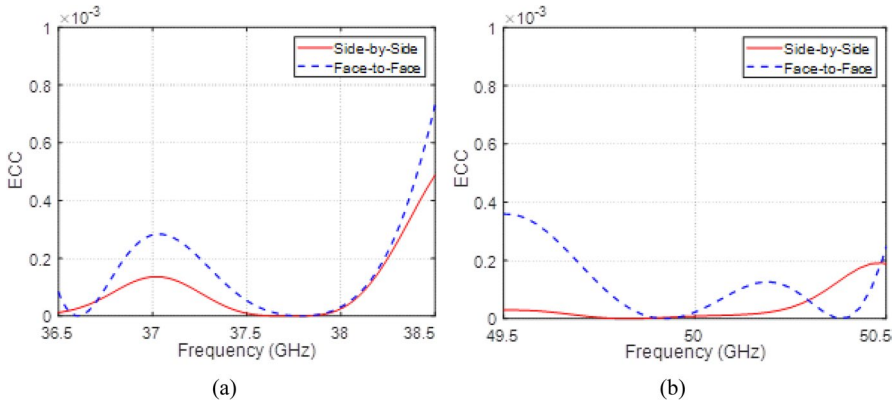
**Fig. 31** Dependence of the ECC of the two-element MIMO antenna on the frequency around (**a**) 37.8 GHz and (**b**) 50 GHz
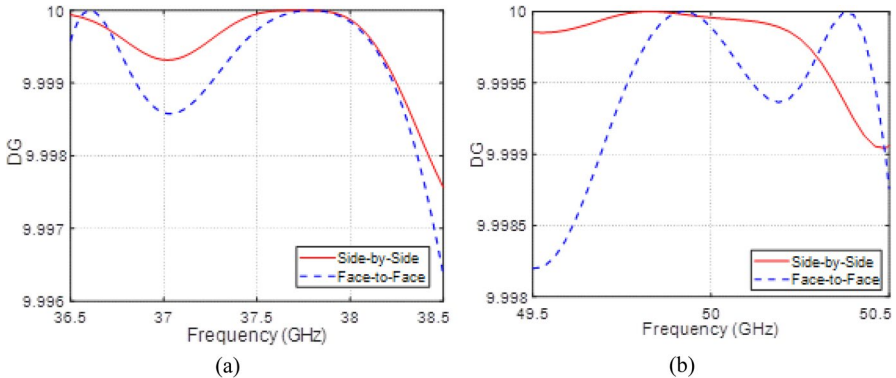
Fig. 32 Dependence of the DG of the two-element MIMO antenna on the frequency around (**a**) 37.8 GHz and (**b**) 50 GHz

### 5.2.2 Two-Element Face-to-Face MIMO Antenna

The MIMO antenna system performance, which is composed of two elements of the CP antenna described in Section 2, is investigated by simulation as well as experimental measurement. The two elements are placed face-to-face, as presented in Figs. 3 and 5c, to produce spatial diversity. The frequency dependence of the reflection coefficient at port 1 is presented in Fig. 23. By comparison between Figs. 23 and 11, it is shown that the frequency response of $|S_{11}|$ of the two-element MIMO antenna is almost identical to that of the single-element antenna. Also, it is shown that the experimental measurements of $|S_{11}|$ come in good agreement with simulation results.
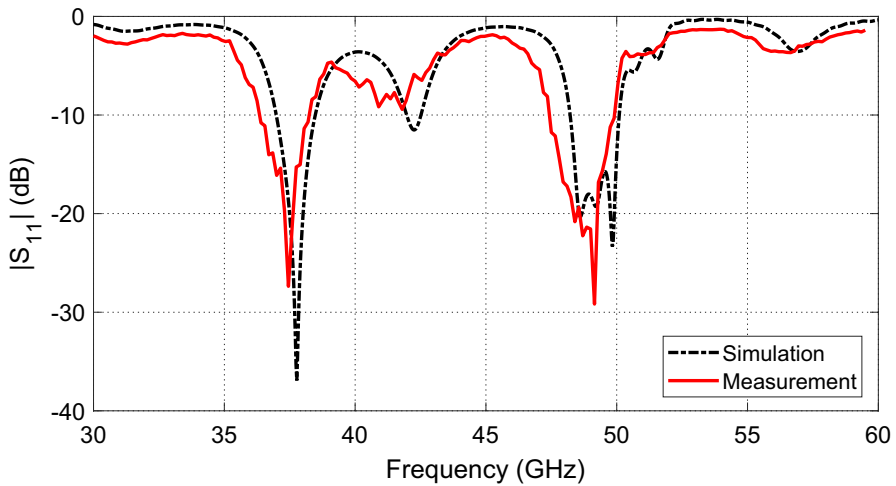
Fig. 33 Variation of $|S_{11}|$, at port 1 of the four-element MIMO configuration with the frequency over a broad frequency band

Fig. 34 Variation of the mutual coupling coefficients, $|S_{21}|$, $|S_{31}|$, and $|S_{41}|$, of the four-element MIMO antenna with the frequency
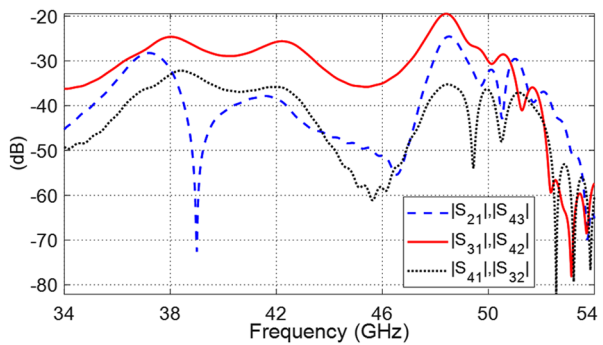

The isolation between the two elements of this MIMO antenna can be measured by the magnitude of the coupling coefficient, $|S_{21}|$, whose frequency response is presented in Fig. 24. The magnitude of the coupling coefficient is maintained below -20 dB over the entire frequency range of investigation showing good performance of the face-to-face MIMO antenna system. As seen, the measurements of $|S_{21}|$ are close to the results obtained by simulation.

The total field radiation patterns of the face-to-face MIMO antenna at 37.8 GHz when fed at ports 1 and 2 are presented in Fig. 25a and b, respectively. The far-field patterns produced at 50 GHz when it is fed at ports 1 and 2 are presented in Fig. 26a and b, respectively. Irrespective of the port of excitation of this MIMO antenna, the values of the peak gain achieved at 37.8 and 50 GHz are 7.6 and 6.55 dBi, respectively.
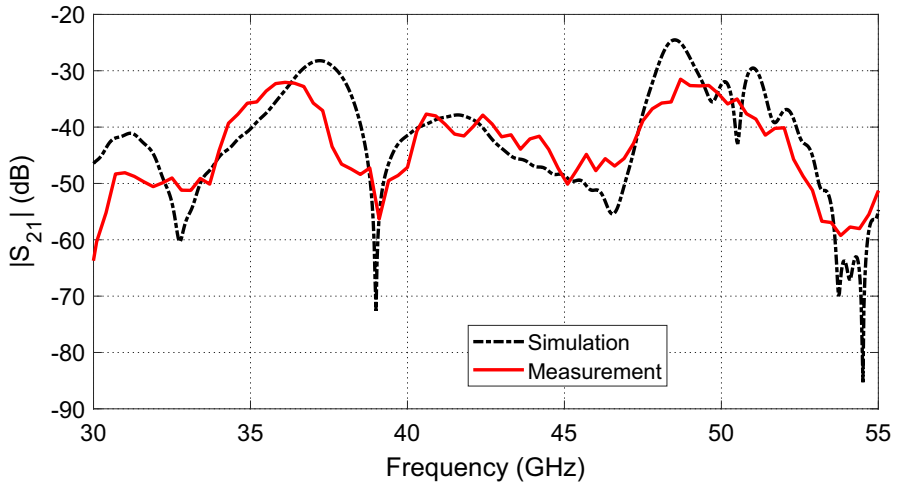
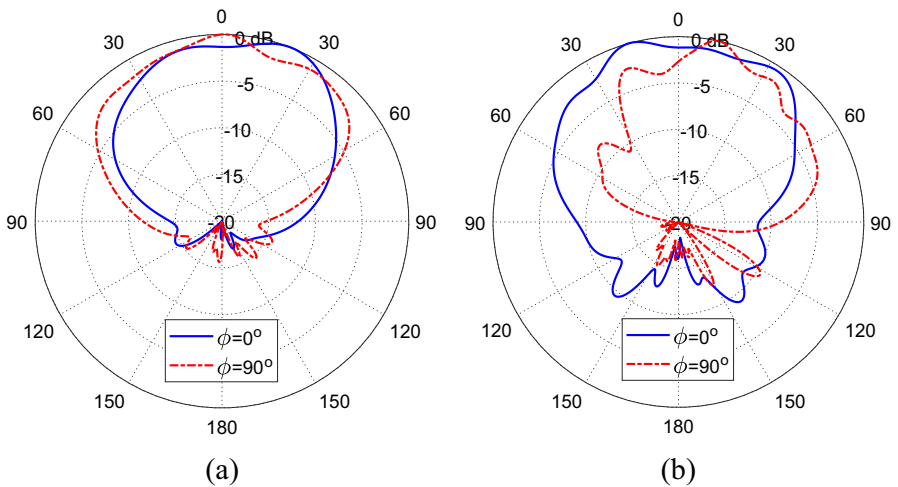**Fig. 35** Variation of the coupling coefficient, $|S_{21}|$, between ports 1 and 2 of the four-element MIMO antenna
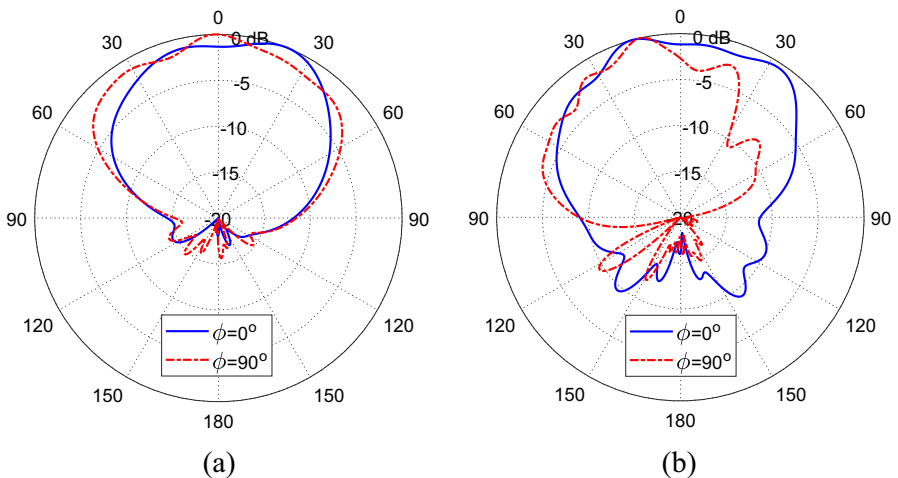
Fig. 36 Radiation patterns of the total field radiated by the four-element MIMO antenna (port 1) at (**a**) 37.8GHz and (**b**) 50 GHz

The patterns of the circularly polarized field components produced by the face-to-face MIMO antenna in the far zone at 37.8 and 50 GHz, are shown in Figs. 27 and 28, respectively, when the MIMO antenna is excited at port 1, and Figs. 29 and 30, respectively, when fed at port 2. It is seen that the far field is mainly RHCP at both the lower and higher frequencies. However, the cross-polarization level of the radiated field at the upper band of frequencies is significantly higher
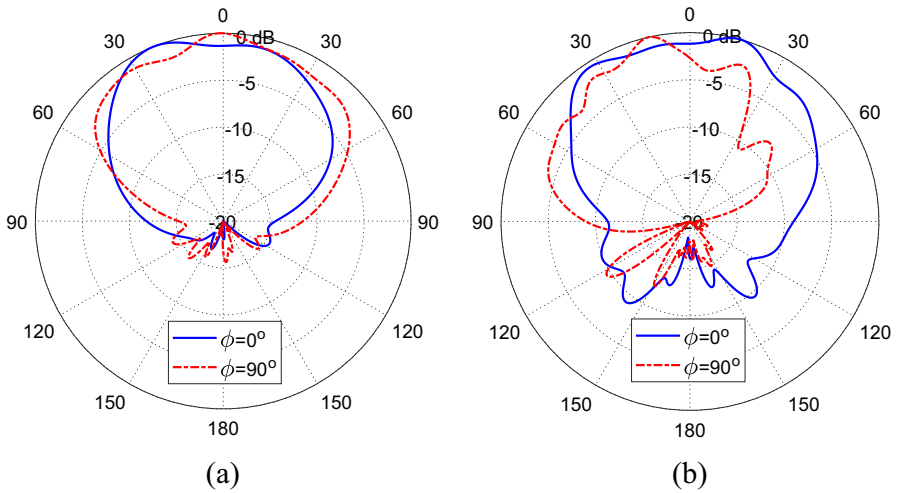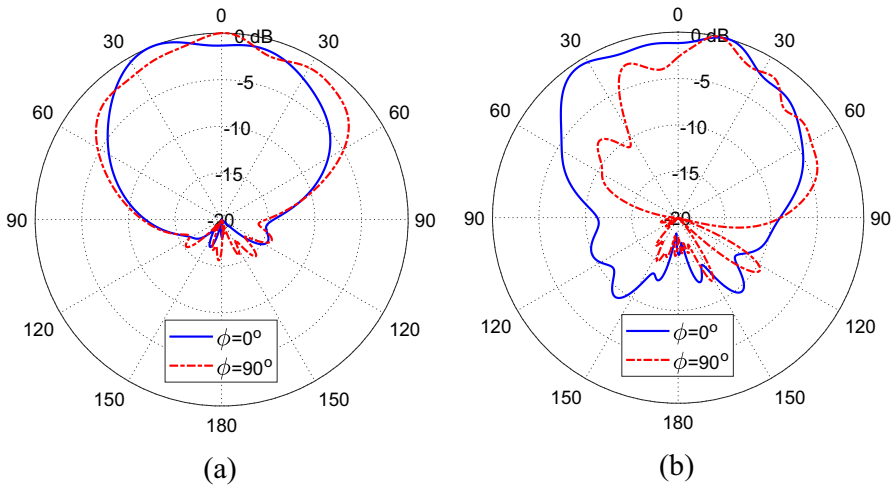
**Fig. 37** Radiation patterns of the total field radiated by the four-element MIMO antenna (port 2) at (**a**) 37.8GHz and (**b**) 50 GHz

Fig. 38 Radiation patterns of the total field radiated by the four-element MIMO antenna (port 3) at (**a**) 37.8GHz and (**b**) 50 GHz

than that of the far field at the lower band of frequencies. This means that the proposed two-element face-to-face MIMO antenna produces more perfect circular polarization at 37.8 GHz that that produced at 50 GHz. This MIMO antenna produces the same type of polarization when fed at port 1 or port 2. Therefore, it can be employed to obtain spatial diversity but not polarization diversity.
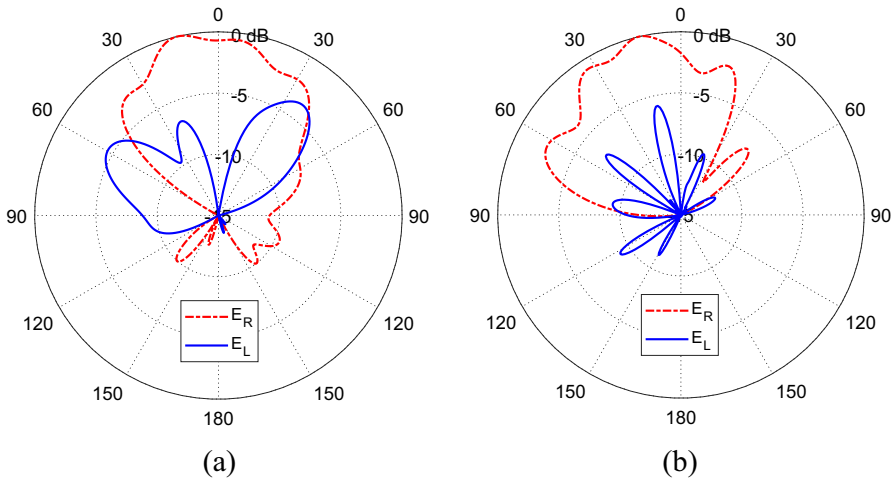
Fig. 39 Radiation patterns of the total field radiated by the four-element MIMO antenna (port 4) at (**a**) 37.8GHz and (**b**) 50 GHz
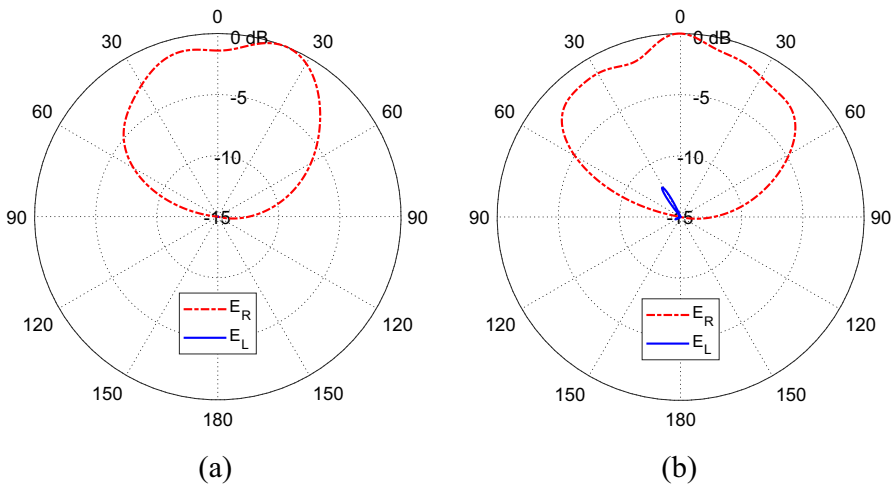
Fig. 40 Radiation patterns of the CP field components (E_R and E_L) of the four-element MIMO antenna (port 1) at 37.8 GHz. **a** $\phi = 0°$. **b** $\phi = 90°$

5.2.3 ECC and DG of the Two-Element MIMO Antennas

The ECC and DG obtained by the side-by-side and face-to-face MIMO antenna configurations are presented in Figs. 31 and 32, respectively, over the operating frequency bands. It is seen that the ECC is very small ($< 10^{-3}$) and the DG is almost 10 over both the frequency bands indicating excellent diversity properties.

Fig. 41 Radiation patterns of the CP field components (E_R and E_L) of the four-element MIMO antenna (port 1) at 50 GHz. **a** $\phi = 0°$. **b** $\phi = 90°$

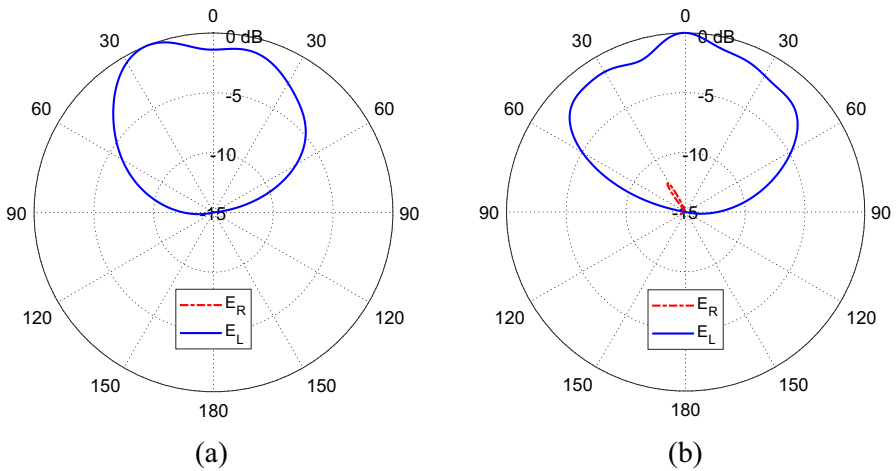**Fig. 42** Radiation patterns of the CP field components (E_R and E_L) of the four-element MIMO antenna (port 2) at 37.8 GHz. **a** $\phi = 0°$. **b** $\phi = 90°$

5.3 Performance Assessment of the Four-Element MIMO Antenna

The four-element MIMO antenna system presented in Fig. 4 is designed to obtain both spatial and polarization diversity. Elements 1 and 4 produce RHCP radiation, whereas elements 2 and 3 produce LHCP radiation.

Fig. 43 Radiation patterns of the CP field components (E_R and E_L) of the four-element MIMO antenna (port 2) at 50 GHz. **a** $\phi = 0°$. **b** $\phi = 90°$

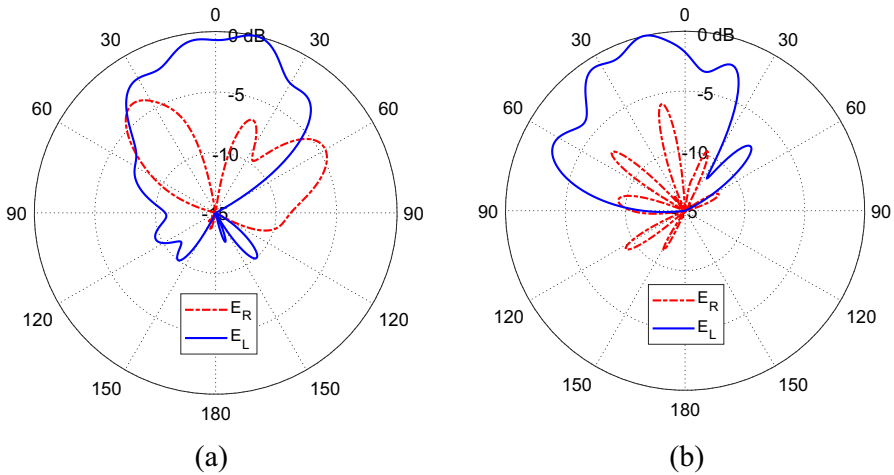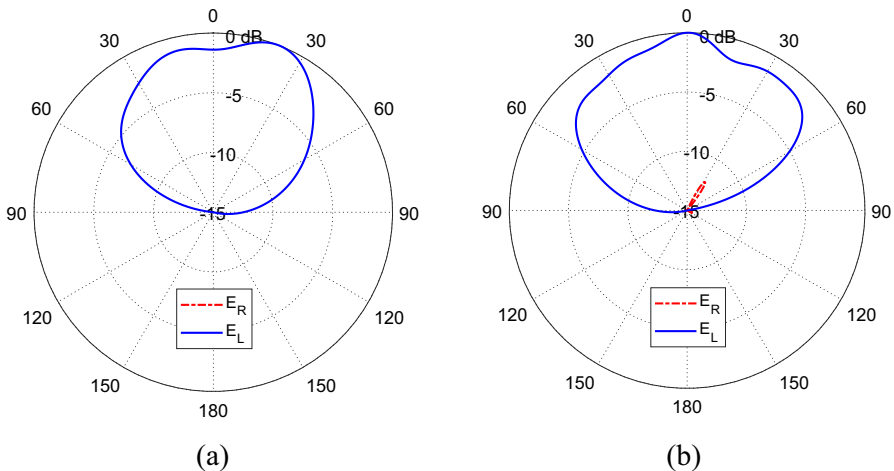**Fig. 44** Radiation patterns of the CP field components (E_R and E_L) of the four-element MIMO antenna (port 3) at 37.8 GHz. **a** $\phi = 0°$. **b** $\phi = 90°$

5.3.1 Mutual Effects between the Elements of the Four-Element MIMO Antenna

The frequency response of $|S_{11}|$ is presented in Fig. 33. The mutual S-parameters of this MIMO antenna are presented in Figs. 34 and 35. By comparing the frequency response of $|S_{11}|$ of the four-element MIMO antenna presented in Fig. 42 to that of the single-element antenna presented in Fig. 11, it is seen that they are

(a)   (b)

Fig. 45 Radiation patterns of the CP field components (E_R and E_L) of the four-element MIMO antenna (port 3) at 50 GHz. **a** $\phi = 0°$. **b** $\phi = 90°$

(a)   (b)
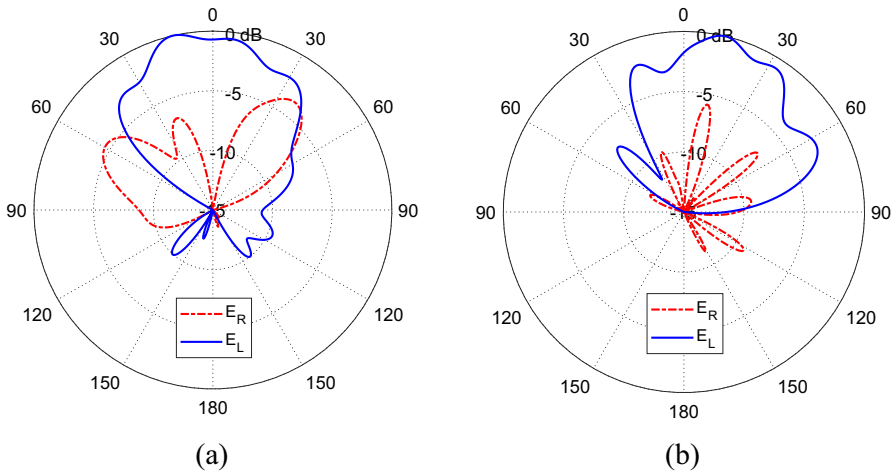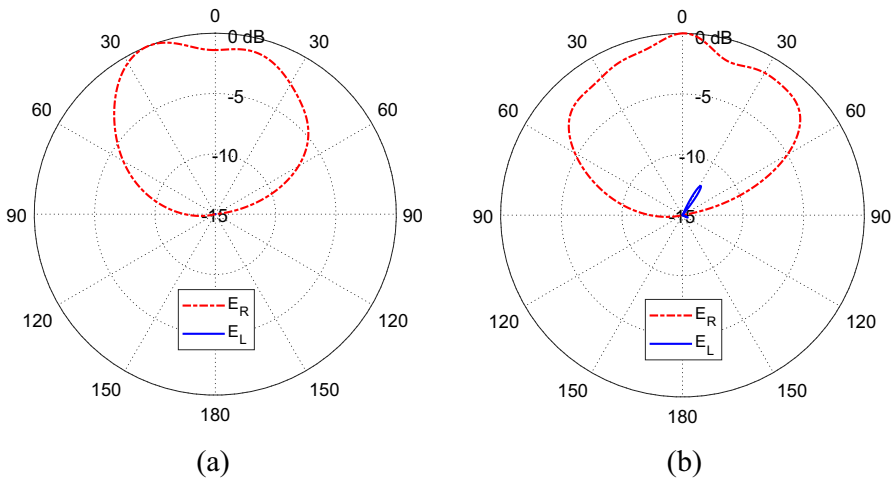
Fig. 46 Radiation patterns of the CP field components (E_R and E_L) of the four-element MIMO antenna (port 4) at 37.8 GHz. **a** $\phi = 0°$. **b** $\phi = 90°$

almost identical. This indicates that the mutual coupling between the elements of the MIMO antenna is very weak, which is emphasized by the frequency responses of the mutual S-parameters presented in Figs. 43 and 44. It is shown that the magnitudes of the mutual S-parameters among the various ports are below -24dB; such low values of the mutual coupling show good isolation between the elements and, hence, excellent diversity is provided by this MIMO antenna.
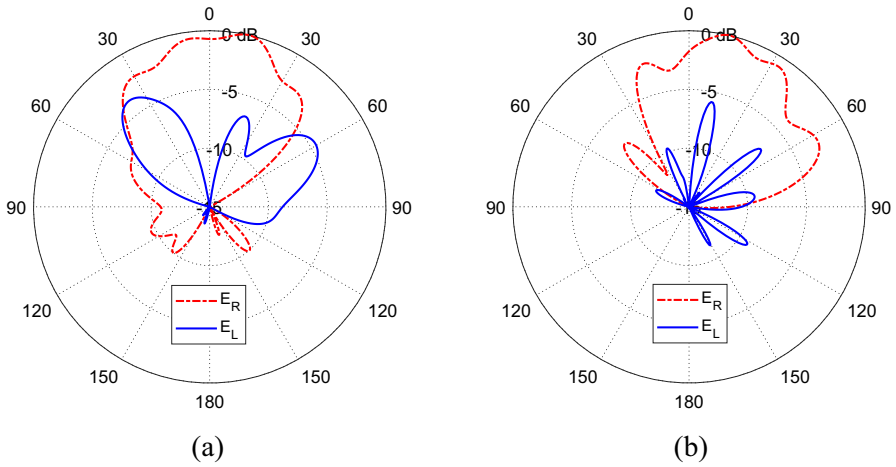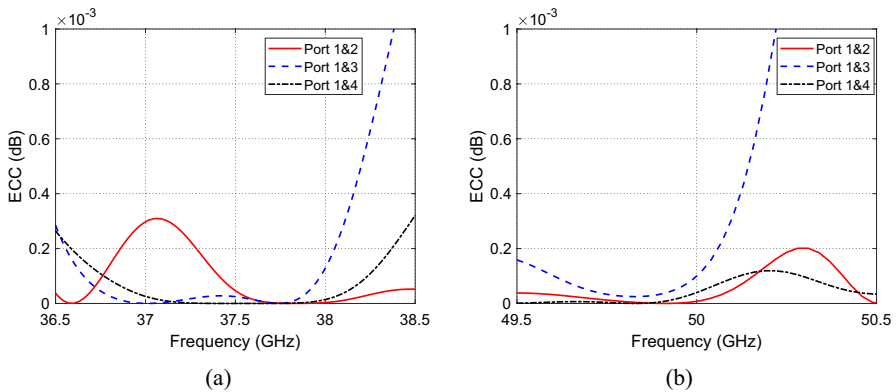
Fig. 47 Radiation patterns of the CP field components (E_R and E_L) of the four-element MIMO antenna (port 4) at 50 GHz. **a** $\phi = 0°$. **b** $\phi = 90°$

Fig. 48 Variation of the ECC of the four-element MIMO antenna with the frequency around (**a**) 37.8 GHz and (**b**) 50 GHz

5.3.2 Radiation Patterns of the Four-Element MIMO Antenna

The radiation patterns of the total field produced by the four-element MIMO antenna when excited at ports 1, 2, 3, and 4 are presented in Figs. 36, 37, 38, and 39, respectively, at the lower and higher operational frequencies of the proposed MIMO antenna.

The radiation patterns of the CP field components radiated by the four-element MIMO antenna when fed at port 1 at the two operating frequencies 37.8 and 50 GHz are presented in Figs. 40 and 41, respectively. The radiation patterns obtained when the antenna is fed at port 2 at the same frequencies are shown in Figs. 42 and 43. Also, the radiation patterns at both frequencies are calculated
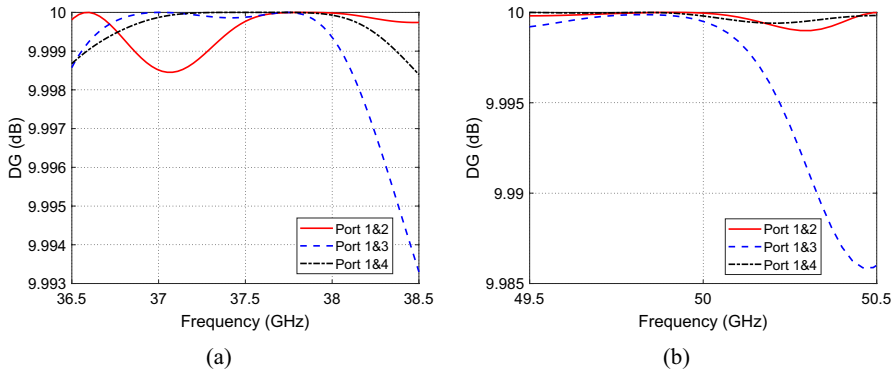
Fig. 49 Variation of the DG of the four-element MIMO antenna with the frequency around (**a**) 37.8 GHz and (**b**) 50 GHz
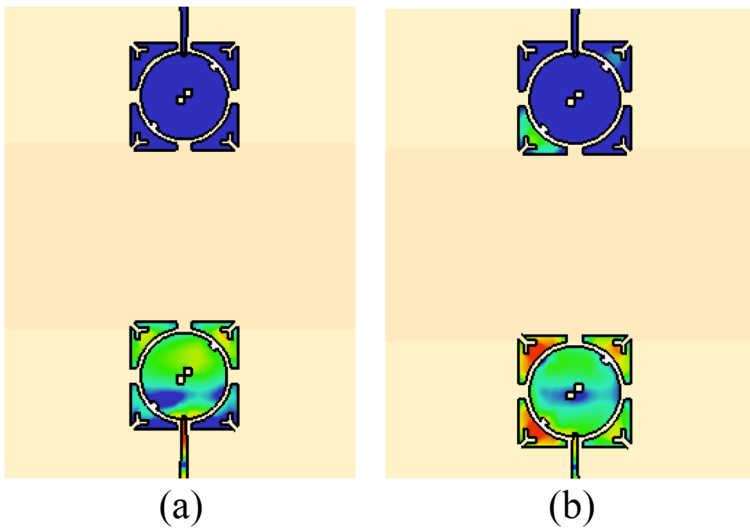
Fig. 50 Surface current distribution over the patches of the face-to-face MIMO antenna system at (**a**) 28 GHz and (**b**) 38 GHz

when the antenna is fed through port 3 and port 4 as illustrated in Figs. 44 and 45, and, Figs. 46 and 47, respectively. It is shown that when port 1 or 4 is used to feed the MIMO antenna, the far field is dominated by RHCP component. On the other side, the far field is dominated by LHCP component when port 2 or 3 is used for feeding the MIMO antenna. It is shown that the cross-polarization level at the higher frequency band is significantly higher than that obtained at the lower frequency band. This means that the four-element MIMO antenna
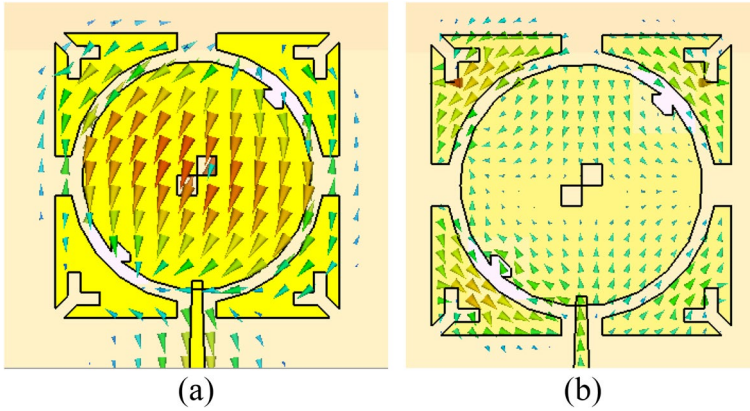
Fig. 51 Surface current distribution over patch 1 of the face-to-face MIMO antenna system at (**a**) 28 GHz and (**b**) 38 GHz

Fig. 52 Surface current distribution over the patches of the side-by-side MIMO antenna system at (**a**) 28 GHz and (**b**) 38 GHz

Fig. 53 Surface current distribution over patch 1 of the side-by-side MIMO antenna system at (**a**) 28 GHz and (**b**) 38 GHz

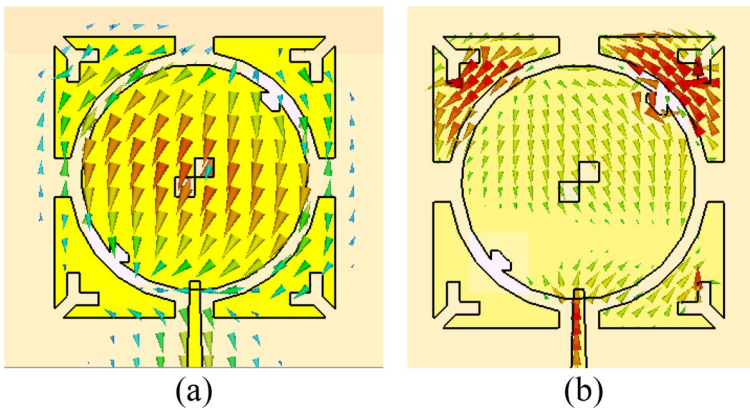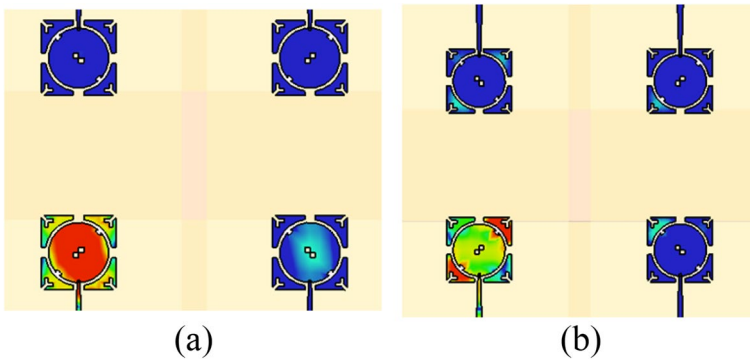**Fig. 54** Surface current distribution over the patches of the four-port MIMO antenna system at (**a**) 28 GHz and (**b**) 38 GHz
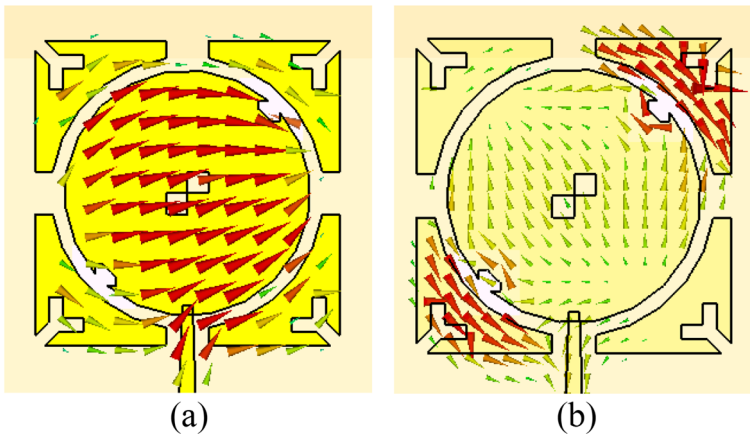
Fig. 55 Surface current distribution over patch 1 of the four-port MIMO antenna system at (**a**) 28 GHz and (**b**) 38 GHz

produces more perfect circular polarization at 37.8 GHz than that produced at 50 GHz. Nevertheless, this MIMO antenna provides polarization diversity in addition to the spatial diversity, where the latter type of diversity is produced owing to the distance between the elements having the same sense of polarization.

5.3.3 ECC and DG of the Four-Element MIMO Antenna

The frequency responses of the ECC and DG of the four-element MIMO antenna are presented in Figs. 48 and 49, respectively, over the operating frequency bands. It is seen that the ECC is very small ($< 10^{-3}$) and the DG is almost 10 over both the frequency bands indicating excellent diversity properties.

Table 2 Comparisons among the perfromance measures of the proposed MIMO antennas and those of other MIMO antennas in previously published papers

Ref	Freq. (GHz)	S_{11} BW (GHz)	Peak G (dBi)	ARBW (dB)	Isolation S_{21} (dB)	ECC (dB)	DG (dB)	No. of elements	Patch dimensions (mm^2)
[9]	28	10	7.3	2.4	< −31	< 0.5	≈ 10	4	3 × 3
[10]	28	0.5	7.3	–	−25	≈ 0	> 9.99	2	4 × 5
	45	1.8	7.03					4	
	51	0.8	7.2						
	56	1	8.03						
[21]	28	0.6	7.38	–	−30	≈ 0	≈ 10	4	4.9 × 5.8
	38	0.6	8.13	–	−40	≈ 0	≈ 10		
[22]	28	0.4	6.9	–	−20	0.1	9.9	2	3.15 × 3.15
[23]	28	5	9.5	–	< −40	< 0.01	> 9.9	4	13 × 15
	38	2.1	11.5	–	< −40	< 0.01	> 9.9		
[24]	28	3.52	7.1	–	−32	≈ 0	≈ 10	4	10 × 10
[25]	28	2.4	8.4	–	> −25	≈ 0	≈ 10	4	4.23 × 2.94
	38	2	6.02	–	> −25	≈ 0	≈ 10		
Present work	37.8	1.499	7.01	0.708	−29	4×10^{-7}	> 9.99	2 side-by-side	2.9 × 2.9
	50	1.855	7.83	0.113	−41.2	8×10^{-6}			
	37.8	1.47	7.61	0.776	−30	5×10^{-8}		2 face-to-face	
	50	1.86	6.58	0.168	−29.2	2×10^{-5}			
	37.8	1.474	7.83	0.708	−29	2×10^{-7}		4	
	50	1.854	7.9	0.129	−44	8×10^{-6}			

5.4 Surface Current Distribution

The surface current distribution over each patch surface has been calculated for all the proposed MIMO configurations. In Fig. 50, the surface current over the face-to-face MIMO antenna system is graphed when port 1 is excited showing very weak coupling between the two antennas. The direction of the current on patch 1 is calculated and plotted in Fig. 51 at both operating bands 28 and 38 GHz. It is clear from Fig. 51 that the antenna exhibits a first-order mode at 28 GHz and second-order mode at 38 GHz.

For the side-by-side MIMO system configuration, the surface current distribution over the elements of the MIMO antennas is shown in Fig. 52 over the two bands 28 and 38 GHz showing very weak coupling at both frequency bands when port 1 is excited. The direction of the surface current is plotted in Fig. 53 on patch 1 at 28 and 38 GHz. By noticing the current distribution on the main patch, it can be seen that a single-order mode is obvious at 28 GHz and second-order mode is shown at 38 GHz.

Finally, the surface current distribution is calculated for the four port MIMO antenna system and demonstrated in Fig. 54 when port 1 is excited, showing low coupling between elements.

The surface current distribution on patch 1 is illustrated in Fig. 55 using arrows to show current direction.

6 Comparison with Previous Work

Comparisons between the performance of the proposed MIMO antennas and that of other MIMO antennas presented in recently published papers are listed in Table 2. These comparisons show some advantages of the proposed MIMO antennas relative to those presented in the other publications. The main advantage of the proposed MIMO antennas is that they provide two bands of circular polarization. Another important advantage over the other published papers is that the proposed four-element MIMO antenna provides two types of diversity (spatial and polarization), whereas the other antennas offer only spatial diversity. The other advantages are the smaller size and high isolation among the multiple ports. However, the main drawback of the proposed MIMO antennas relative to other published designs is the narrow bandwidth. Nevertheless, the two frequency bands achieved by the proposed MIMO antennas can be considered wide enough for operation in applications of future wireless communication.

7 Conclusion

A novel CP low-profile printed antenna has been designed to produce circular polarization over two frequency bands around 37.8 and 50GHz. Two-element side-by-side and face-to-face MIMO antenna configurations have been proposed to attain spatial diversity. A four-element MIMO antenna has been proposed to achieve both spatial and polarization diversity at the same time. The proposed dual-band CP single-element, two-element MIMO, and four-element MIMO antennas have been fabricated

for experimental study. Both the numerical and experimental investigations have shown that the mutual coupling between any two ports of the proposed MIMO antennas is below -25dB. Also, for any two ports it has been shown that the ECC is below 1×10^{-7} and the diversity gain is higher than 9.99. The impedance matching bandwidths (for $|S_{11}| < -10$dB) have been shown to be 1.53 and 1.88 GHz at 37.8 and 50GHz, respectively, and the corresponding 3-dB axial ratio bandwidths have been shown to be 700 and 130MHz, respectively.

Data Availability Data sharing not applicable to this article as no datasets were generated or analyzed during the current study.

Declarations

Competing Interests The authors declare no competing interests.

References

1. A. K. Dwivedi, A. Sharma, A. K. Singh, and V. Singh. Design of dual band four port circularly polarized MIMO DRA for WLAN/WiMAX applications. Journal of Electromagnetic Waves and Applications, vol. 34, no. 15, pp. 1990-2009, 2020.
2. W. A. Li, Z. H. Tu, and Q. X. Chu. Compact, high isolation, and dual-polarized differential dual-notched UWB-MIMO slot antenna. Microwave and Optical Technology Letters, vol. 57, no. 11, pp. 2609-2614, 2015.
3. A. E. Farahat and K. F. A. Hussein. 28/38 GHz dual-band Yagi-Uda antenna with corrugated radiator and enhanced reflectors for 5G MIMO antenna systems. Progress In Electromagnetics Research C, vol. 101, pp. 159-172, 2020.
4. M. M. M. Ali, and A. R. Sebak, "Design of compact millimeter wave massive MIMO dual-band (28/38 GHz) antenna array for future 5G communication systems", 17th International Symposium on Antenna Technology and Applied Electromagnetics (ANTEM), pp. 1-2, 2016.
5. H. S. Fang, C. Y. Wu, J. S. Sun, and J. T. Huang. Design of a compact MIMO antenna with pattern diversity for WLAN application. Microwave and Optical Technology Letters, vol. 59, no. 7, pp. 1692-1697, 2017.
6. Z. Wani, M. P. Abegaonkar, and S. K. Koul. A 28-GHz antenna for 5G MIMO applications. Progress In Electromagnetics Research Letters, vol. 78, pp. 73-79, 2018.

7. P. Sambandam et al. Integration of slot array with MIMO antenna for 4G and 5G applications. Wireless Personal Communications, vol. 109, no. 4, pp. 2719-2731, 2019.
8. M. N. Hasan, S. Bashir, and S. Chu. Dual band omnidirectional millimeter wave antenna for 5G communications. Journal of Electromagnetic Waves and Applications, vol. 33, no. 12, pp. 1581-1590, 2019.
9. A. M. Saleh, K. R. Mahmoud, M. M. Elmesalawy, and I. I. Ibrahim, "2x2 MIMO Wideband Circularly Polarized Patch Antenna Array for 5G Millimeter-Wave Systems", International Conference on Computer Communication and Informatics (ICCCI), pp. 1-5, 2021.
10. M. Abd Abo-Elhassan, A. E. Farahat, and K. F. A. Hussein. Compact-size quad-band patch and MIMO antenna system for 5G mobile handsets. Progress in Electromagnetics Research C, vol. 112, pp. 221-238, 2021.
11. D. G. Patanvariya, and A. Chatterjee, "A Compact Triple-Band Circularly Polarized Slot Antenna for MIMO System", International Symposium on Antennas and Propagation (APSYM), pp. 54-57, 2020.
12. P. Muthusamy, K. C. R. Madaka, P. K. Chaitanya, and N. Srikanta, "Polarized Diversity Characteristics Dual-Band MIMO Antenna for 5G/WLAN Applications" , Proceedings of the International Conference on Paradigms of Communication, Computing and Data Sciences (PCCDS), pp. 169-177, 2022.
13. G. Saxena, Y. K. Awasthi, and P. Jain, "Four-element pentaband MIMO antenna for multiple wireless application including dual-band circular polarization characteristics" , International Journal of Microwave and Wireless Technologies , Vol. 14, No. 4, pp. 465-476, 2022.
14. S. S. Singhwal, B. K. Kanaujia, A. Singh, J. Kishor, and L. Matekovits. Dual-band circularly polarized MIMO DRA for sub-6 GHz applications. International Journal of RF and Microwave Computer-Aided Engineering, vol. 30, no. 10, p. e22350, 2020.
15. G. Bharti, D. Kumar, A. K. Gautam, and A. Sharma. Two-port dual-band circularly polarized dielectric resonator-based MIMO antenna with polarization diversity. Electromagnetics, vol. 40, no. 7, pp. 463-478, 2020.
16. M. Hussain, I. A. Awan, A. Mazhar, S. N. R. Rizvi, M. Alibakhshikenari, F. Falcone, and E. Limiti, "A Simple Low-Profile Broadband Antenna Design for 5G Millimeter-Wave Applications Over 38 GHz Spectrum", MTT-S Latin America Microwave Conference (LAMC), pp. 1-4, 2021.
17. M. Hussain, I. A. Awan, S. M. Rizvi, M. Alibakhshikenari, F. Falcone, and E. Limiti,, "Simple Geometry Multi-Bands Antenna for Millimeter-Wave Applications at 28 GHz, 38 GHz, and 55 GHz Allocated To 5G Systems", 46th International Conference on Infrared, Millimeter and Terahertz Waves (IRMMW-THz), pp. 1-2, 2021.
18. M. Hussain, I. A. Awan, S. M. Rizvi, M. Alibakhshikenari, F. Falcone, and E. Limiti, "Design and fabrication of a printed tri-band antenna for 5G applications operating across Ka-, and V-band spectrums" , Electronics, Vol. 10, No. 21, 2021.
19. I. A. Awan, M. Hussain, S. N. R. Rizvi, M. Alibakhshikenari, F. Falcone, and E. Limiti, "Single Patch Fractal-Shaped Antenna with Small footprint Area and High Radiation Properties for Wide Operation Over 5G Region" , 46th International Conference on Infrared, Millimeter and Terahertz Waves (IRMMW-THz), pp. 1-2, 2021.
20. G. Saxena, P. Jain, and Y. K. Awasthi. High diversity gain MIMO-antenna for UWB application with WLAN notch band characteristic including human interface devices. Wireless Personal Communications, vol. 112, no. 1, pp. 105-121, 2020.
21. R. R. Elsharkawy, K. F. A Hussein, and A. E. Farahat. Dual-band (28/38 GHz) compact MIMO antenna system for millimeter-wave applications. Journal of Infrared, Millimeter, and Terahertz Waves 44, no. 11, pp. 1016-1037, 2023.
22. M. Usman, E. Kobal, J. Nasir, Y. Zhu, Chao Yu, and A. Zhu, "Compact SIW Fed Dual-Port Single Element Annular Slot MIMO Antenna for 5G mmWave Applications" , IEEE Access, Vol. 9, 2021.
23. M. Hussain, W. A. Awan, E. M. Ali, M. S. Alzaidi, M. Alsharef, D. H. Elkamchouchi, A. Alzahrani and M. Fathy Abo Sree. Isolation improvement of parasitic element-loaded dual-band MIMO antenna for mm-wave applications. Micromachines, Vol. 13, Art. No. 1918, 2022.
24. M. Hussain, E. M. Ali, S. M. R. Jarchavi, A. Zaidi, A. I. Najam, A. A. Alotaibi, A. Althobaiti and S. S. M. Ghoneim. Design and characterization of compact broadband antenna and its MIMO configuration for 28 GHz 5G applications. Electronics, vol. 11, Art. No. 523, 2022.
25. A. D. Tadesse, O.P. Acharya, and S. Sahu. A compact planar four-port MIMO antenna for 28/38 GHz millimeter-wave 5G applications. Advanced Electromagnetics, Vol.11, No.3, pp.16–25, 2022.

Publisher's Note Springer Nature remains neutral with regard to jurisdictional claims in published maps and institutional affiliations.

Authors and Affiliations

Nada Alaa[1] · Rania A. Elsayed[1] · Asmaa E. Farahat[2] · Khalid F. A. Hussein[2] · Walid S. El-Deeb[1]

✉ Asmaa E. Farahat
  e_asma_e@yahoo.com

  Nada Alaa
  engnadaalaa@gmail.com

  Rania A. Elsayed
  en_rania_helika@yahoo.com

  Khalid F. A. Hussein
  fkhalid@eri.sci.eg

  Walid S. El-Deeb
  wseldeeb@ucalgary.ca

[1] Electronics and Communications Engineering Department, Faculty of Engineering, Zagazig University, Zagazig, Egypt

[2] Microwave Engineering Department, Electronics Research Institute, Cairo 11843, Egypt